



Cairo University

AIAA Design | Build | Fly 19 - 20

Design Report

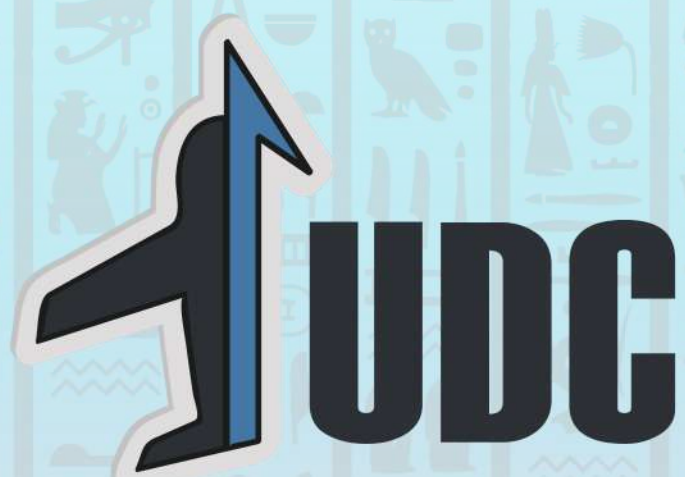


Table of Contents

1.0 Executive Summary	4
1.1 DESIGN PROCESS	4
1.2 PERFORMANCE AND CAPABILITIES OF THE DESIGN	4
3.0 Conceptual Design	6
3.1 MISSIONS REQUIREMENTS	6
3.1.2 <i>General Constraints</i>	8
3.2 KEY DESIGN PARAMETERS	8
3.2.1 <i>Score Sensitivity Analysis</i>	9
3.2.2 <i>Translation into Design Requirements</i>	12
3.3 CONFIGURATIONS EXPLORED	12
3.3.1 <i>Fuselage Configuration</i>	14
3.3.2 <i>Propulsion System</i>	15
3.3.3 <i>Banner Mechanism</i>	15
3.4 FINAL CONCEPTUAL DESIGN	16
4.0 Preliminary Design	17
4.1 DESIGN METHODOLOGY	17
4.2 DESIGN TRADES	17
4.2.1 <i>Constraints Sizing</i>	17
4.3 MISSION MODEL	19
4.3.1 <i>Description and Capabilities</i>	19
4.3.2 <i>Uncertainties</i>	20
4.4 AERODYNAMIC CHARACTERISTICS	20
4.4.1 <i>Airfoil Selection</i>	20
4.4.2 <i>High-Lift Devices</i>	21
4.4.3 <i>Drag Calculation</i>	22
4.5 STABILITY AND CONTROL	27
4.5.1 <i>Longitudinal Static Stability</i>	27
4.6 MISSION PERFORMANCE ESTIMATIONS	31
5.0 Detail Design	31
5.1 DIMENSIONAL PARAMETERS	31
5.2 STRUCTURAL CHARACTERISTICS AND CAPABILITIES	32
5.2.1 <i>Layout and Design</i>	32
5.2.2 <i>Flight Envelope</i>	32
5.3 SUB-SYSTEMS DESIGN AND INTEGRATION	33
5.3.1 <i>Wing structure</i>	33
5.3.2 <i>Fuselage design</i>	33
5.3.3 <i>Landing gear</i>	36
5.3.4 <i>Empennage</i>	36
5.3.5 <i>Receiver and Transmitter Selection</i>	36
5.3.6 <i>Servo Selection</i>	37
5.3.7 <i>Propulsion System</i>	37
5.4 WEIGHT AND BALANCE	38
5.5 FLIGHT AND MISSION PERFORMANCE	40
5.5.1 <i>Flight performance</i>	40
6.0 Manufacturing Plan	45

6.1 MANUFACTURING PROCESSES INVESTIGATED	45
6.2 SELECTED MANUFACTURING PROCESS	45
6.2.1 <i>Wing</i>	45
6.2.2 <i>Fuselage and Tail Structure</i>	46
6.2.3 <i>Mechanisms</i>	47
6.2.4 <i>Banner</i>	47
6.3 MANUFACTURING MILESTONE	47
7.0 Testing Plan	48
7.1 TESTING SCHEDULE	48
7.2 SUBSYSTEMS TESTING OBJECTIVES	48
7.2.1 <i>Propulsion Testing</i>	48
7.2.2 <i>Structural Testing</i>	49
7.2.3 <i>Banner Testing</i>	50
7.3 FLIGHT TESTING	51
7.4 FLIGHT CHECKLISTS	51
8.0 Performance	52
8.1.1 <i>Propulsion System Battery</i>	52
9.0 Bibliography	55

Acronyms, Abbreviations, and Symbols

AR_h	Horizontal Tail Aspect Ratio	S	Wing Area
AR	Aspect Ratio	S_{ref}	Reference Surface Area
AoA	Angle of Attack	S_{wet}	Wetted Area
CAD	Computer Aided Design	S_g	Take-off Ground Roll Distance
CG	Center of Gravity	S_h	Horizontal Tail Surface Area
CL	Lift Coefficient	S_v	Vertical Tail Surface Area
CD	Drag Coefficient	SM	Static Margin
CL_{max}	Maximum Lift Coefficient	T	Thrust
CD_0	Parasite Drag Coefficient	UDC	Unmanned Aerial Vehicles Development Centre
C_f	Skin Friction Coefficient	V_h	Horizontal Tail Volume
C_R	Root Chord	V_v	Vertical Tail Volume
C_m	Moment Coefficient	V_{cruise}	Cruise Speed
C_m	Moment Coefficient	V_{stall}	Stall Speed
D	Drag Force	V_{turn}	Turn Speed
ESC	Electronic Speed Controller	V_{pack}	Package Voltage
FOM	Figure of Merits	W	Aircraft Weight
FF	Form Factor	W/S	Wing Loading
GM	Ground Mission	a	Acceleration
I_{max}	Maximum Electric Current	b	Wing Span
L	Lift Force	e	Oswald efficiency
$(\frac{L}{D})_{Max}$	Maximum Lift to Drag Ratio	l_h	Horizontal Tail Arm
$(\frac{L}{D})_{cruise}$	Lift to Drag Ratio During Cruise	$(\frac{t}{c})_{max}$	Maximum Thickness to Chord Ratio
M_1	Flight Mission 1	t_2	Time to Double Amplitude
M_2	Flight Mission 2	$t_{1/2}$	Time to Half Amplitude
M_3	Flight Mission 3	μ	Friction Coefficient
MAC	Mean Aerodynamics Chord	λ	Taper Ratio
Lipo	Lithium polymer	ζ	Damping Ratio
$NiMh$	Nickel Metal Hydride	ω_n	Undamped Natural Frequency
NP	Neutral Point	ω_d	Damped Frequency
Q	Interference Factor		
Re	Reynold's Number		
RPM	Revolutions Per Minute		

1.0 Executive Summary

This report details the design, manufacturing, and testing processes of an aircraft for the 2019-2020 AIAA Design/Build/Fly (DBF) competition by the Cairo University, Unmanned aerial-systems Development Center (UDC) team. The objective of this year's competition is to develop an unmanned radio-controlled banner towing bush plane. The aircraft with a maximum wingspan of 5 ft should be capable of externally carrying a stowed banner, remotely deploying and towing it during flight and remotely releasing the banner before landing. Additionally, the aircraft should be capable of performing a charter flight by completing three laps while carrying as number of passengers along with their luggage in the least time possible.

1.1 Design Process

The design process started with the team investigating the effect of the banner on the aircraft to find a reliable method for calculating the banner drag. Subsequently, several trade studies and sensitivity analyses have been conducted to determine the effect of various design parameters on the score. It was deduced that the speed of the aircraft is of highest impact on the team's score and overall performance. Accordingly, the team's self-imposed requirement has been the development of the fastest aircraft.

In order to design for a high speed, analyses have been conducted on the banner design and the propulsion during the conceptual phase. The aircraft take-off weight and aerodynamics characteristics were then estimated in preliminary design phase. Wind tunnel tests were performed to determine the best banner design that minimize the banner fluttering and drag. Extensive effort has been also put into the selection of a propulsion system that delivers the dynamic thrust needed at the desired flight-speed.

1.2 Performance and Capabilities of the Design

The designed aircraft is capable of successfully completing 3 laps while carrying 18 passengers with their luggage as payload. As well as, towing of a 120-inch-long banner for 5 successive laps which can be remotely deployed and released. The aircraft capabilities have been confirmed during six successful flight tests.



Figure 1.1 Final Aircraft

2.0 Management Summary

2.1 Team Organization

The 2019-2020 Cairo university's DBF team consists of 15 undergraduate students; two seniors, six sophomores and seven juniors. The eight elder team members have participated in the previous competitions while the new ones were carefully selected after winning the annual UDC DBF local competition. The team works under the supervision of our faculty advisors with continuous guidance and support from the mentoring chief engineer. This team structure was selected to combine knowledge, experience and creativity allowing for the continuity and development of the team.

The team is managed by an elected team member who handles the team logistics, assign tasks and deadlines for each sub-team and links between the students and the faculty advisors. A weekly meeting is held to discuss the project progress, propose ideas and take decisions.

2.2 Management Chart

The team was further divided into 8 parallel sub-teams, each sub-team has a leader who is responsible for distributing the workload among the sub-team members and reporting the sub-team progress to the team leader.

Figure 2.1 illustrates our team hierarchy and the assignment areas for each member. However, it only serves as an outline as all team members work together and help each other to achieve the objective of the team.

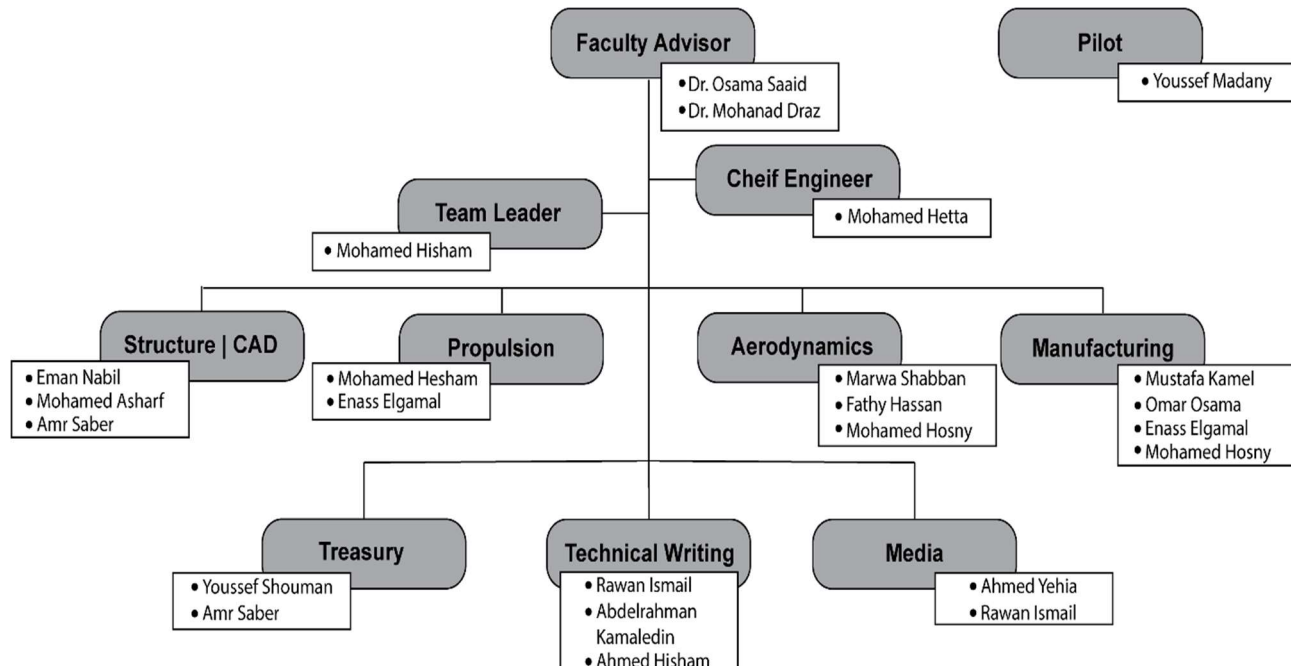


Figure 2.1: Team Structure

2.3 Milestone Chart

A Gantt chart shown in figure 2.2 was conducted to highlight the important phases and milestones of the competition and the planned versus the actual progress of the team. Sticking to those deadlines allowed for the development and optimization of several prototypes.

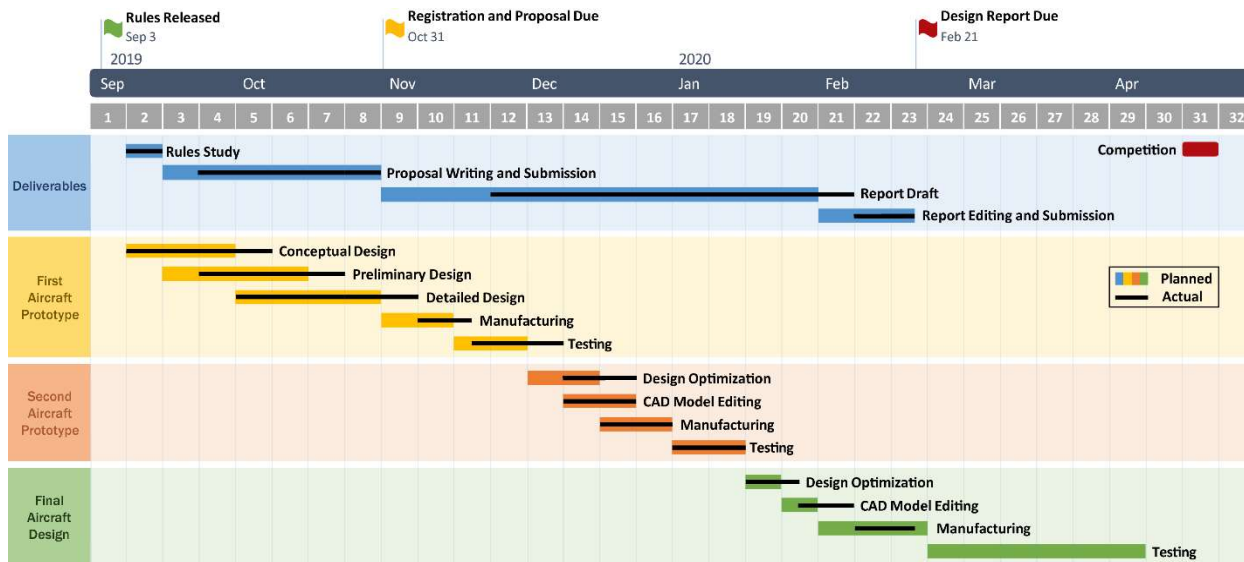


Figure 2.2: Milestones Gantt chart

3.0 Conceptual Design

The conceptual design process was initiated by analyzing the 2020 rules and determining the design parameters affecting the score, which were converted into Figures of Merit and used to compare several design options and configurations. The output of this design phase was a complete and clear concept for the aircraft that would best maximizes our chance of winning the competition.

3.1 Missions Requirements

The main objective of this year is to design a banner towing bush plane. The plane with a maximum allowable wingspan of 5 *feet* must also be capable of carrying passengers and their luggage.

The aircraft performance is tested through three flight missions and one ground mission. The final score of each team is calculated according to equation 3.1.

$$Score = Written\ Report\ Score * Total\ Missions\ Score \quad (3.1)$$

Where the total mission score is the sum of the individual flight missions and the ground mission, and is calculated according to equation 3.2.

$$Total\ Mission\ Score = M1 + M2 + M3 + GM \quad (3.2)$$

All Flight missions will take the path shown in figure 3.1, which consists of two 1000 *ft.* straight paths one of them is downwind while the other in upwind in addition to two 180-degree turns and a 360-degree turn. In order for a mission to be considered successful, it must be concluded with a successful landing without any damage or bouncing off the runway upon touchdown.

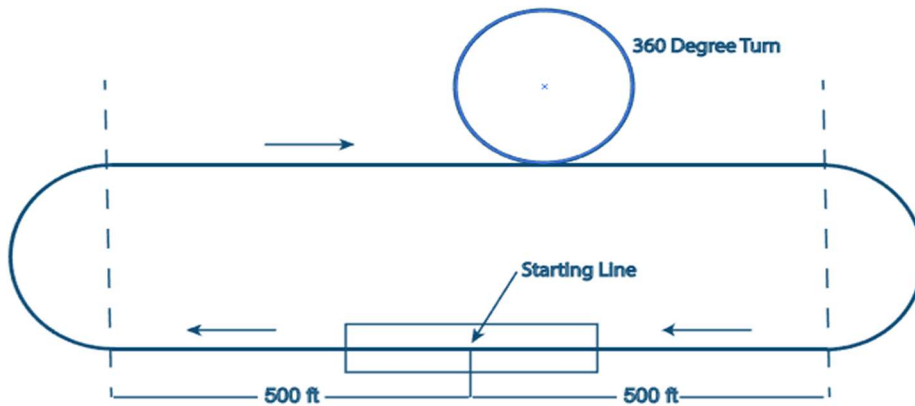


Figure 3.1: Course Layout

Flight Mission 1: Test Flight

The unloaded aircraft must takeoff within a 20 *feet* ground roll field length, complete 3 laps, and perform a successful landing for the mission to be considered successful. The flight window for this mission is 5 minutes. This is a pass/fail mission with the score shown in equation 3.3.

$$M1 = 1 \text{ (if successful)} \quad (3.3)$$

Flight Mission 2: Charter Flight

For a maximum flight window of 5 minutes, the aircraft should carry the passengers and their luggage, complete 3 laps, and perform a successful landing. This mission favors the carrying of many passengers and completing the mission in minimal time. The score for this mission is calculated according to equation 3.4.

$$M2 = 1 + \frac{\left(\frac{\# \text{Passengers}}{\text{time}} \right)_N}{\left(\frac{\# \text{Passengers}}{\text{time}} \right)_{\max}} \quad (3.4)$$

Flight Mission 3: Banner Flight

For a flight window of 10 minutes, the aircraft loaded with the banner must takeoff within a 20 *feet* ground roll field length, deploy the banner on the downwind leg of the pattern, tow the banner for as many laps as it could, release the banner upon crossing the finish line of the last lap, and finally perform a successful landing.

This mission favors the completion of many laps and towing a long banner. The mission score is calculated according to equation 3.5.

$$M3 = 2 + \frac{(\# \text{laps} \times \text{banner length})_N}{(\# \text{laps} \times \text{banner length})_{\max}} \quad (3.5)$$

Ground Mission: Operational Demonstration

The ground mission is intended to test the reliability and the ease of accessibility of the designed aircraft through complete ground demonstrations of missions 2 and 3. The ground mission is timed, and the score is calculated according to equation 3.6.

$$GM = \frac{Min_{time}}{N_{time}} \quad (3.6)$$

The ground mission scenario starts with the crew member loading the aircraft with the passengers and their luggage. The crew member then returns to the mission box, removes the passengers and luggage, and proceeds to install the banner in the stowed configuration onto the aircraft. This would conclude the timed portion of the mission. The assembly crew member will then hold the aircraft in the vertical position with the tail down, and the pilot will then demonstrate the flight controls are active and then demonstrate both the deployment and release of the banner.

3.1.2 General Constraints

In addition to the mission requirements, the aircraft design must comply with some additional constraints.

Propulsion System:

- Batteries can be either NiCad/NiMH or LiPo. However, the total stored energy cannot exceed 200 watt-hours.
- Individual LiPo battery packs cannot exceed 100 watt-hours per pack [FAA limit for hand carry on commercial flights].

Sizing:

- The maximum allowable wingspan for the aircraft is 5 *feet*.

Banner Design:

- The banner maximum aspect ratio is 5, and its minimum length is 10 *inches*.
- Deployment and release must be done remotely in flight.

3.2 Key Design Parameters

The general rules and the specific mission requirements were carefully analyzed in order to interpret them and identify the key design parameters, as shown in table 3.1.

Table 3.1: Design Requirements

Missions		Mission Requirements / Objectives	Key Design Parameters
Ground Mission		<ul style="list-style-type: none"> • Fast installing & removing of the passengers and luggage. • Reliable banner mechanism. 	<ul style="list-style-type: none"> • Time
Flight Missions	Mission 2	<ul style="list-style-type: none"> • Complete 3 laps in minimal time. • Carrying the passengers and luggage as payload. 	<ul style="list-style-type: none"> • Speed/Propulsion Power • Number of Passengers
	Mission 3	<ul style="list-style-type: none"> • Takeoff within a 20 <i>ft.</i> ground roll field length. • Complete maximum number of laps towing a long banner. • Remote deployment and releasing of the banner. 	<ul style="list-style-type: none"> • Takeoff Distance • Banner Length & Drag • Number of Laps/Endurance

3.2.1 Score Sensitivity Analysis

Analyzing the scoring criteria showed that the main design parameters are the **number of passengers** as it affects the aircraft's total weight, and the **banner length** which mainly affects the drag of the aircraft. Other scoring parameters such as the time of the charter flight mission and the number of laps in the banner flight mission are both dependent parameters on the chosen number of passengers and banner length. The following analysis expresses these relations mathematically and investigates the effect of the main design parameters on the total score.

Mission 2

For mission 2, the weight of each passenger along with their luggage is 5 oz. ($\approx 0.142\text{ Kg.}$), which were rounded up to 0.15 Kg. per passenger to account for the weight of the passenger seat and luggage room. Equation 3.9 describes the weight as a function of number of carried passengers.

$$W_{Mission\ 2} = W_{Mission\ 1} + W_{payload} \quad (3.7)$$

$$\therefore W_{payload} = 0.15 \times N_{passengers} \quad (3.8)$$

$$\therefore W_{Mission\ 2} = W_{Mission\ 1} + 0.15 \times N_{passengers} \quad (3.9)$$

During cruise, the aircraft performance is governed by equation 3.10 bellow, from the simple $Thrust = Drag$ and $Lift = Weight$ assumptions during cruise [...].

$$T = \frac{1}{2} \rho V_{cr}^2 S \times \left[C_{D_0} + \frac{(2W_{Mission\ 2}/\rho \cdot V_{cr}^2 \cdot S)}{\pi e AR} \right] \quad (3.10)$$

Solving equations 3.9 and 3.10 for the cruise speed (V_{cr}) at different values of number of passengers, results in an estimate of the cruising time of mission 2 as a function of the number of carried passengers, which was plotted into figure 3.2.

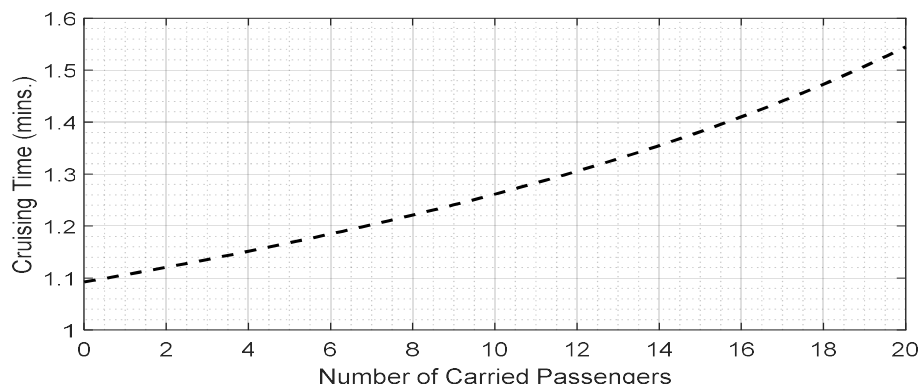


Figure 3.2: Effect of Passengers on the Cruise Time

Mission 3

The length of the towed banner in mission 3 directly sets the cruising speed of the aircraft during the mission. Equation 3.11 is an empirical estimate of the drag coefficient of a polyester fabric banner based on [...].

$$C_{d_{banner}} = 0.012 + \frac{0.016}{Width \times Length \times g} \times 0.39 \times AR_{banner}^{-1.25} \quad (3.11)$$

While the banner drag can be calculated for a certain speed by equation 3.12.

$$D_{banner} = C_{d_{banner}} \times Length \times Width \times \rho \times V^2 \quad (3.12)$$

Referenced to our aircraft, the banner drag coefficient would be,

$$C_{D_{banner}} = \frac{D_{banner}}{\frac{1}{2} \times \rho \times S_{ref} \times V^2} \quad (3.13)$$

During cruise, equation 3.10 can be rewritten into equation 3.14.

$$T = \frac{1}{2} \rho V_{cr}^2 S \times \left[C_{D_0} + C_{D_{banner}} + \frac{(2W_{Mission3}/\rho \cdot V_{cr}^2 \cdot S)}{\pi e AR} \right] \quad (3.14)$$

Solving equation 3.14 for the cruise speed at different values of banner length while keeping the banner aspect ratio constant ($AR_{banner} = 5$), we can arrive at an estimate of the cruise time and hence an approximate estimate for the number of laps performed. This relation is plotted into figure 3.3.

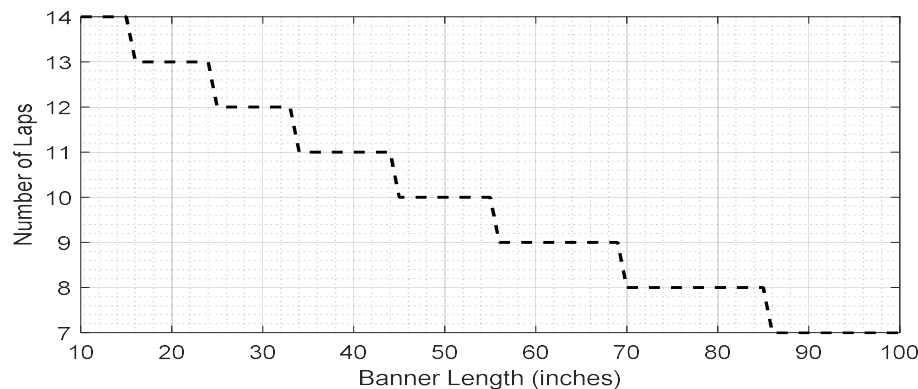


Figure 3.3: Effect of the Banner Length on the Number of Laps

Combined Analysis

Starting with a reasonable range for the **banner length** and the **number of passengers**, the corresponding number of laps in the banner flight mission and the time of the charter flight mission were calculated and taken into account to calculate the total score.

Figure 3.4 shows the percentage change of the total score against the effect of changing the parameters. Results showed that the parameters of this year have a little numerical effect on the total score. It also

appears that there is no contradiction between both parameters, and that the winning aircraft is the one that carries the most passengers and tows the longest banner. Although, it appears that the number of passengers would have slightly more effect on the total score than the banner length.

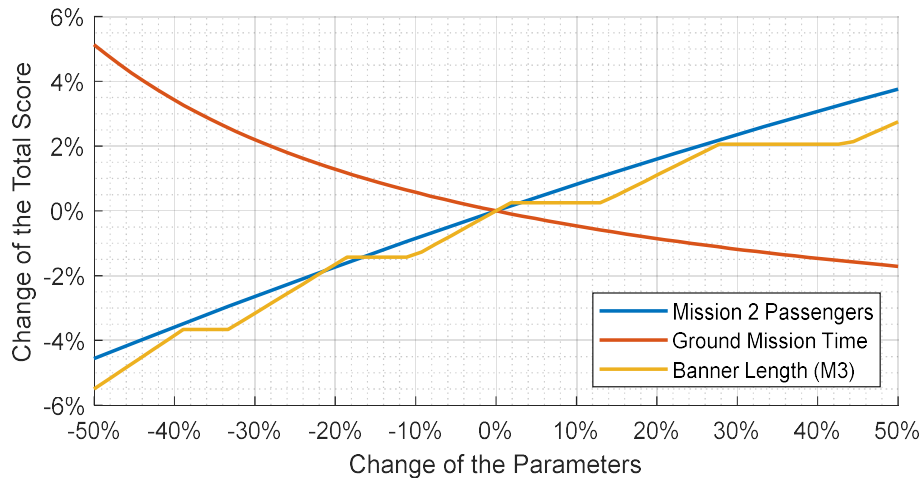


Figure 3.4: Sensitivity of the Total Score to the Change in design Parameters

Various scenarios for the design parameters have been calculated and plotted with their corresponding score into figure 3.3, which also shows the selected values for the parameters and the estimated score based on the predicted range for the parameters.

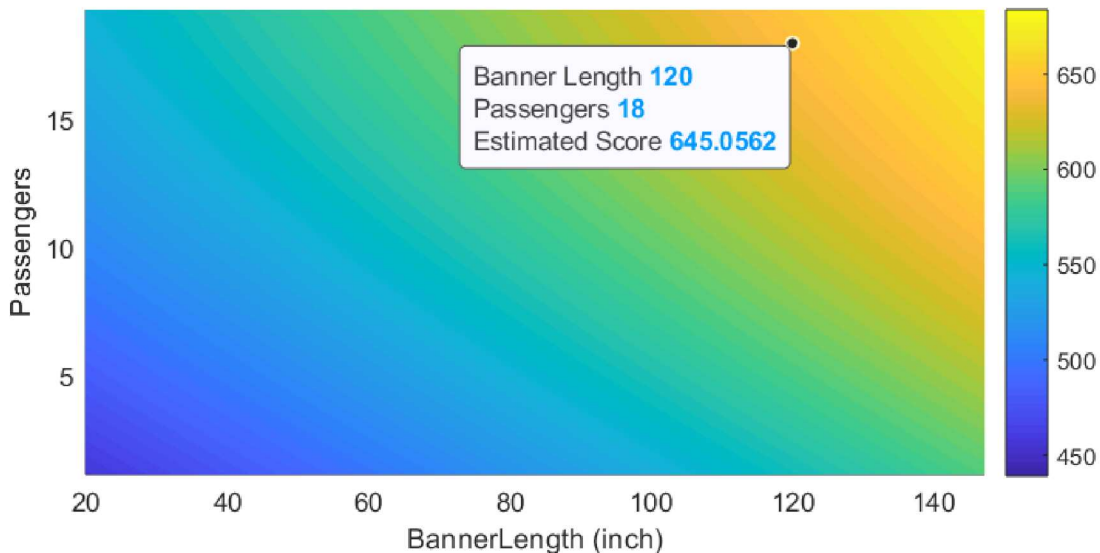


Figure 3.5: Estimated Score of Various Design Scenarios

We have chosen the selected values for the key design parameters shown in figure 3.5 as we think that succeeding in building an aircraft with this performance values will lead to us winning the competition. These values represent what we think is the limit of the “reasonable design region” for this edition of the DBF competition.

3.2.2 Translation into Design Requirements

The previous analysis of the scoring system determined the most important parameters to be considered. The targeted mission performance of this aircraft is as shown in table 3.2.

Table 3.2: Desired Performance

Mission 2 Carried Passengers	18
Mission 2 Time (s)	90
Mission 3 Length of Towed Banner (in)	120
Mission 3 Number of Laps	5

The following design requirements represent what we think is necessary in order to achieve the targeted performance in table 3.2.

- Flight Speed: It was considered as the most important design requirement for this year, as it affects both the number of scoring laps for mission 3 and the time for mission 2. This translates into designing for very low drag, minimizing the banner drag and maximizing the propulsion system power / dynamic thrust.
- Payload Capacity: It's targeted that the aircraft carries 18 passengers during the second mission. This means that the aircraft's empty weight should be minimized in order to have the capacity to carry more passengers. Accordingly, light configurations will be favored.
- Stability: The aircraft must be able to withstand disturbances caused upon the deployment of the banner and due to banner fluttering. An unstable plane would have a hard time towing a long banner.
- Mechanical Simplicity: Simplicity of various mechanisms and the ease of loading is significant for the ground mission.

3.3 Configurations Explored

Several design options for each of the aircraft components were proposed by the team members. To organize and facilitate the process of assessing each configuration, the following matrix of alternatives shown in table 3.3 was created.

Table 3.3: Matrix of Design Alternatives

Component	Design Alternatives			
	Conventional	Biplane	Blended Wing-Body	Flying-Wing
Wing	Conventional	Biplane	Blended Wing-Body	Flying-Wing
Empennage	Conventional Tail	U-Tail	Inverted U-Tail	Inverted V-tail
Tail Attachment	On Fuselage	Single Boom	Twin Booms	
Propulsion	Single Tractor	Double Tractor	Single Pusher	
Landing Gear	Taildragger	Tricycle		

Out of the created matrix of design alternatives three complete aircraft configurations were proposed by the team members as viable solutions to this year's design problem. The configurations as shown in figure 3.6 are: (1) conventional single tractor with twin booms and inverted U-tail, (2) flying-wing configuration, and (3) biplane configuration with a conventional tail.

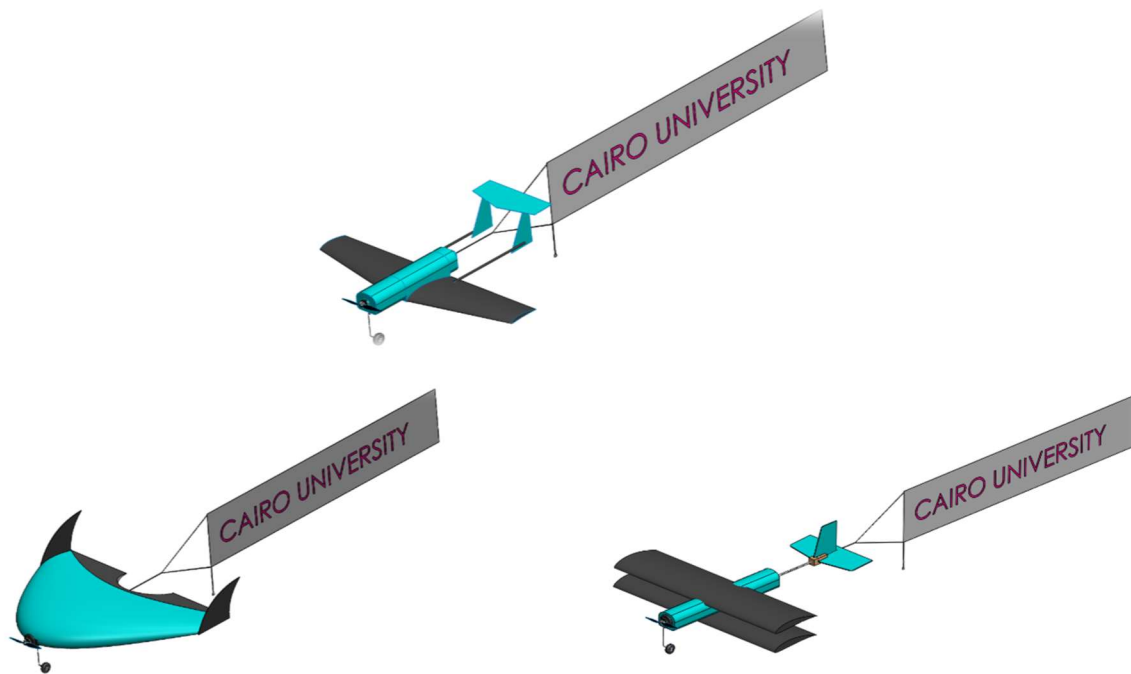


Figure 3.6: Configurations Explored

In order to assess each configuration, the design requirements were translated into five major figures of merit to choose between the proposed configurations. Table 3.4 lists the figures of merit and their weight which reflects their importance to the scoring system on a scale from 1 to 5.

Table 3.4: Figures of Merit

Figure of Merit	Weight
Speed & Drag	5
Weight	5
Stability	4
Payload Capacity	3
Simplicity	2

The biplane configuration would double the wing surface area, hence, it would have the lowest wing loading out of all other configurations, which would mean carrying a lot of passengers and performing the missions with minimal power loading required. However, a biplane would have significantly higher drag, and is usually a slow-flyer configuration.

A flying wing configuration would have the lowest drag out of all proposed configurations, which means that it would be the fastest, however, it falls behind in terms of the stability and the payload capacity. Which will prevent us from carrying a lot of passengers inside.

The conventional configuration represents the middle ground between both the flying wing and the biplane configurations. It possesses good stability traits due to the tail control surfaces; it also features low drag and a high payload capacity.

In order to finalize and conclude the previous discussion on the aircraft configurations, a figure of merits analysis was performed. Each configuration was assessed on a scale ranging from 0 to 5, which was then multiplied by the FOM weight. The configuration with the highest total score was selected. Table 3.5 shows the figure of merit analysis for the three configurations discussed earlier.

Table 3.5: Figure of Merit Analysis

Aircraft Configurations				
FOM	Weight	Conventional	Flying Wing	Biplane
Speed & Drag	5	3	5	1
Weight	5	4	4	3
Stability	4	5	2	4
Payload Capacity	3	4	2	4
Simplicity	2	4	5	3
Total		75	69	54

3.3.1 Fuselage Configuration

After choosing the main aircraft configuration, Analysis were conducted to compare and evaluate the three considered fuselage designs shown in table 3.6. The main objective was to find a configuration that can fulfil the structure requirements while having the least drag to maximize the aircraft curving speed. The total drag of each configuration was estimated using FlightStream for missions two, three and the take-off which will be detailed in section 4.4.3. It was found that the round edged conventional fuselage design exerted the least drag and hence was chosen for the final design.

Table 3.6 Considered fuselage designs

Fuselage Configurations				
FOM	Weight	Sharp Edged [Box]	Round Edged	Lifting Body
Speed & Drag	5	3	5	2
Weight	5	5	4	3
Stability	4	5	5	5
Payload Capacity	3	5	5	2
Simplicity	2	5	5	3
Total		85	90	57

3.3.2 Propulsion System

Regarding the propulsion configuration, pusher designs were excluded to avoid the possibility of interfering with the towed banner during the third mission, as this scenario is very likely to occur while performing turns and maneuvers.

Table 3.6: Propulsion Configuration FOM

Propulsion Configurations			
FOM	Weight	Single Tractor	Double Tractor
Speed & Drag	5	5	4
Weight	5	5	3
Stability	4	3	5
Payload Capacity	3	3	5
Simplicity	2	5	3
Total		81	76

Both the single and double tractor configurations were considered as shown in table 3.6. Although, the twin motor design would provide higher static thrust during takeoff which is beneficial, the efficiency of this design is generally worse than having a single large motor due to increased losses. While the only disadvantage of the single tractor configuration was the torque exerted on the aircraft due to the spiral flow on resulting from the rotation of the propeller. This was later solved by initially deflecting the rudder while moving on the runway to compensate for the yawing effect. Hence, the single tractor configuration was favored and chosen as the final propulsion system configuration.

3.3.3 Banner Mechanism

The banner mechanism needs to deploy and release the banner during flight. Two main concepts for the banner mechanisms has been proposed by the structure sub-team members. In the first concept, the banner is kept in place using two elastic rubber threads that are kept in tension using two servo motors mounted on opposite sides of the fuselage. The other concept proposed to alternate the rubber bands with grippers. However, the gripper mechanism was found to encounter severe dynamic flight loads moreover it was more complex. Figure 3.6 shows the chosen concept.

Upon moving the servo motors, the threads are released and so is the banner. The banner is attached to the bottom of the fuselage using a third servo motor, which is also used to release the banner.

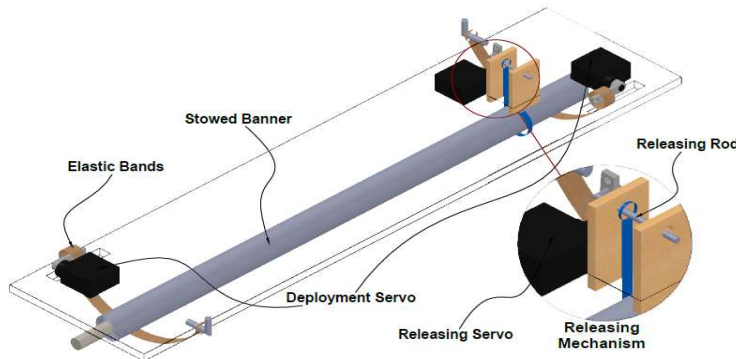


Figure 3.6: Banner Mechanism Concept

3.4 Final Conceptual Design

Based on the former discussion and the figure of merit analysis of the aircraft configurations, the final configuration selected, shown in figure 3.7, is a low-wing, twin boom, single tractor with a high-fixed conventional tail (inverted U). This concept would allow for enough clearance for the banner which will be towed from a point underneath the fuselage. The final conceptual design is designed to carry 18 passengers and their luggage in a compartment inside the fuselage, and would be capable of towing an 120-inch banner.

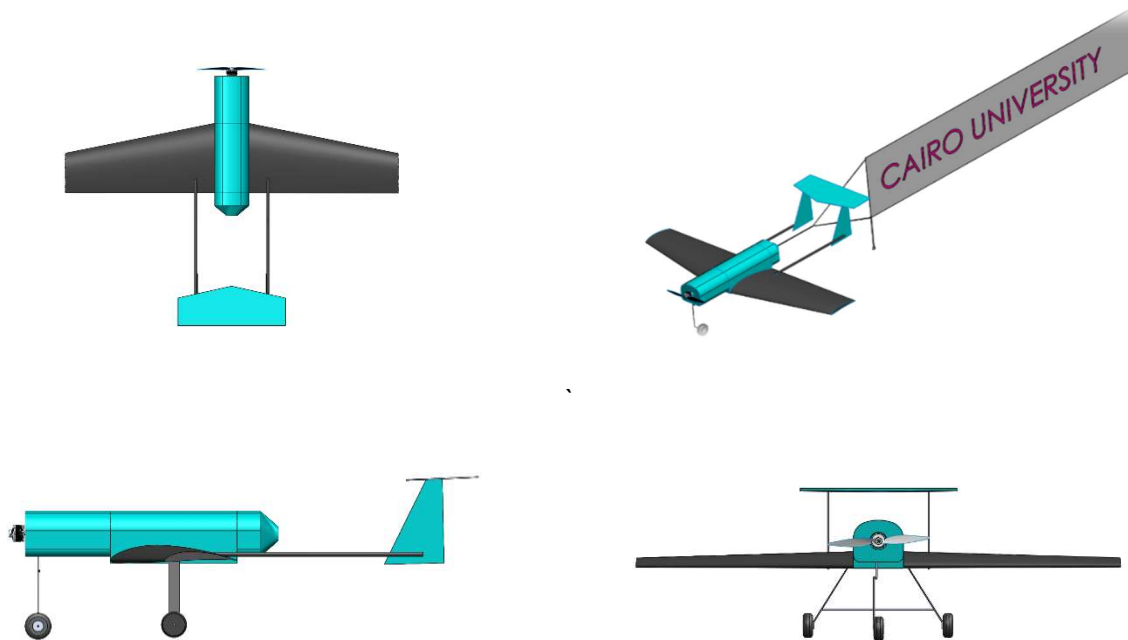


Figure 3.7: Final Conceptual Design

4.0 Preliminary Design

The main objectives of this phase were to further shape and optimize the conceptual aircraft design based on the trade studies and missions model analysis. Hence, a matching plot was conducted to find the optimum design point, predict the aircraft mission performance and maximize the score through an iterative process.

4.1 Design Methodology

After translating the mission requirements into design requirements and constraints in the prior section, the mission performance was estimated using a matching plot with the take-off distance, cruise and stall speeds as the main constraints. Consequently, the optimum design point that yields the highest score was chosen.

Afterwards, the propulsion, aerodynamics and stability trades were conducted inducing the initial sizing of each sub-system. An iterative process took place as shown in figure 4.1 aiming for maximizing the cruise speed while minimizing the empty weight and total drag of the aircraft to allow for the carriage of the maximum number of passengers and towing the longest banner possible.

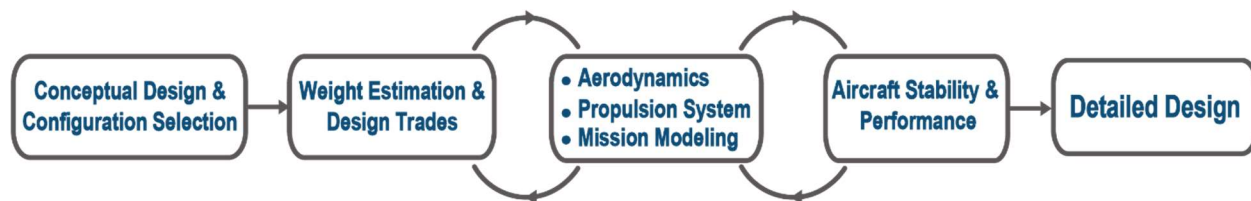


Figure 4.1 Flowchart of the Design methodology

4.2 Design Trades

4.2.1 Constraints Sizing

The main constraints obligated by this year missions were the take-off distance being 20 feet in both mission 1 and 3. In addition, maximizing the aircraft cruise speed was vital for achieving a maximum score. Considering the mentioned constraints, a matching plot was conducted defining the take-off distance, cruise speed and stall speed which were set on the conceptual phase.

Hence, the relation between the wing loading and power to weight ratio was plotted using the appropriate performance equations as shown in figure 4.2. This constraint analysis shaped the shaded feasible design area that ensures meeting all mission requirements and the optimal design point was chosen.

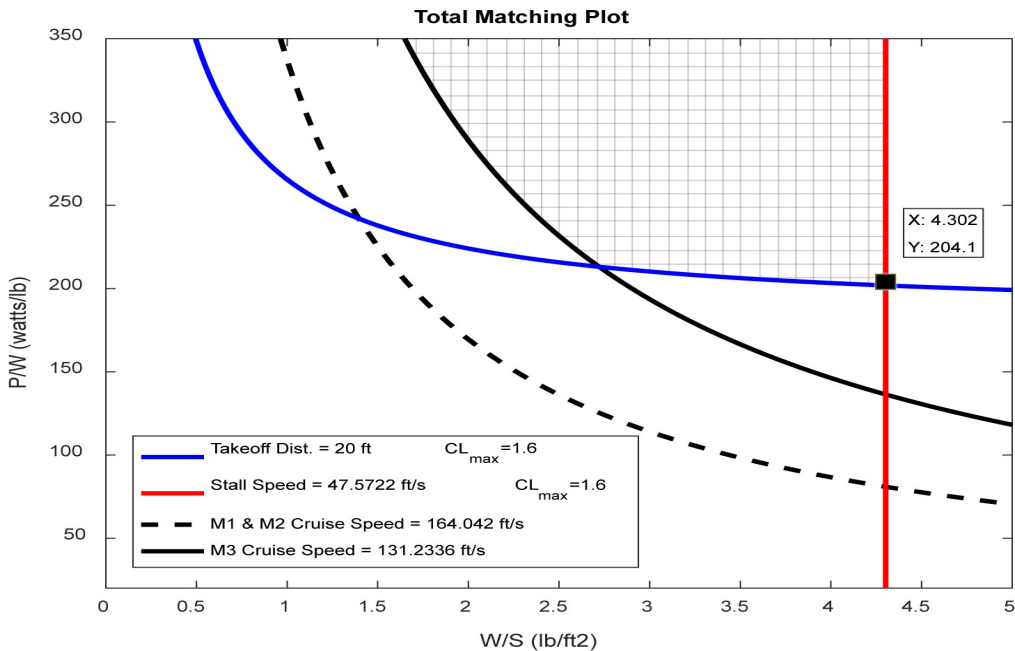


Figure 4.2 Constraints Diagram

Knowing the aircraft maximum take-off weight estimation [19.841 lb], the power and wing area required for satisfying the design requirements were calculated and summarized in table 4.1 below.

Table 4.1 Design Point Values

Parameter	Value
Wing Loading (W/S) [psf]	4.3
Power to Weight Ratio (P/W) [Watts/lb]	204.1
Wing Area (S) [ft ²]	4.84
Power Required (P) [Watts]	4049.5

4.2.2 Propulsion System Selection

The propulsion system was designed to minimize the time required to complete three laps in mission 2 with the maximum payload and allowing for the maximum number of laps to be flown while towing the longest banner possible in mission three. Sizing for mission 3 was prioritized as it implies towing the longest banner as well as flying as many laps as possible in ten minutes.

Allowing the usage of LiPo batteries was considered to be of a huge advantage and was immediately chosen over all other types of batteries as it has much higher specific energy which will allow for faster and larger aircrafts that are capable of carrying more payload. Moreover, the team has a wide experience in using and handling of this type of batteries.

After putting our design restraints and conducting the matching plot, the required thrust for takeoff, cruise and overcoming the drag of the banner was calculated. More than 800 combinations of different motors and a range of APC electric propellers varying in diameter from 10 in to 20 in were compared in terms of

static thrust using eCalc software. A special tool was developed by our team members that facilitates the usage of the official APC Propellers ® database to determine the thrust of a certain propeller at various airspeeds and RPMs [1].

With the maximum propulsion power being limited to 200 watt-hours, several combinations of cells with different endurance were considered. It was found that a total of two 12 cell packs having 2250 capacity each and connected in parallel is the best combinations that fulfills our requirements. Table 4.2 shows the top performing systems that were selected for further testing.

Table 4.2 Top Preforming Propulsion Systems

Motor	<i>Kv</i>	Battery Cells	Current (Amps)	Propeller	Static Thrust (lb)	System Weight (lb)
KDE700XF-545-G3	535	2 × 12 cell 2250 mAh LiPo packs	150	APC 12x8	28.44	5
Scorpion HKII-4225	550	2 × 12 cell 2250 mAh LiPo Packs	145.5	APC 12x8	30.3	4.72
Hacker A50-10L Tornado	530	2 × 9 cell 2250 mAh Lipo packs	140.7	APC 14x8.5	26.1	4.86

4.3 Mission Model

4.3.1 Description and Capabilities

The different missions were modeled in order to predict the anticipated score and performance of the aircraft. Each flight mission can be simplified into four main stages as shown in figure 4.3.

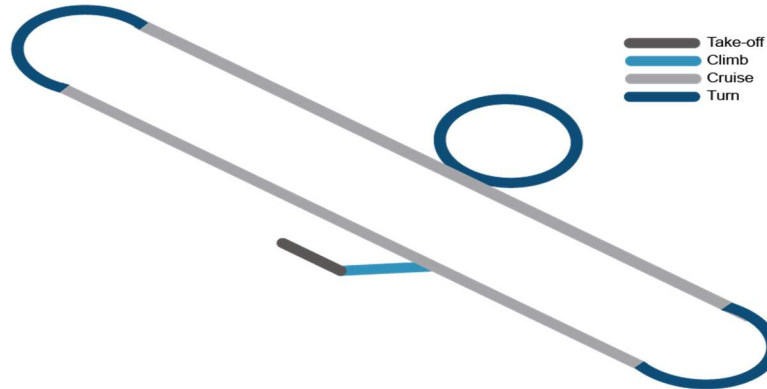


Figure 4.3 Mission Model

- 1. Take-off:** The ground roll distance in both mission 1 and 3 is 20 ft. The aircraft takes off at the maximum motor throttle and constant AoA. The takeoff speed was assumed to be 1.1x of the aircraft stall speed.
- 2. Climb:** The aircraft climbs to a safe altitude which was taken to be 150 ft above the ground level assuming constant rate of climb and angle of attack.

3. Cruise: un-accelerated steady flight at maximum lift to drag ratio with the drag equal to the thrust and the lift equal to the weight.

4. Turn: The mission model consists of two 180° turns and one full 360° turn. The speed, altitude and turning rates were assumed to be constant during the turn.

4.3.2 Uncertainties

There are several limitations and uncertainties to the previous model due to some factors that can't be entirely controlled during the mission. Some of the main uncertainties in our mission model are stated below:

- **Wind:** The wind conditions weren't considered in the above model which may lead to loss in altitude due to head and cross winds. The difference in weather between the competition site and our testing site was estimated based on historical data. However, the results remain uncertain.
- **Propulsion System:** The propulsion system efficiency and endurance are highly dependent on the wind conditions, altitude and temperature. Hence, the thrust and drag calculations will vary depending on those conditions.
- **Banner:** The banner fluttering and behavior can't be fully predicted throughout the mission course. It's also uncertain that the banner will always remain vertical specially during turns. Moreover, there is a probability that the banner may get stuck or tangled during deployment or release.
- **Human Error:** It's assumed that the pilot is capable of operating the aircraft at its optimal conditions during all phases of the mission including landing at slightly high speeds.

4.4 Aerodynamic Characteristics

4.4.1 Airfoil Selection

Using an airfoil that possesses the desirable aerodynamic characteristics needed for this year's missions greatly helps in making the aircraft more efficient. As we are focused on building a fast aircraft, the airfoil was selected not only to have a high $C_{L_{max}}$ value, but also to induce as low drag as possible and to require as low pitching moment as possible. Simplicity of manufacturing was also taken into consideration, and airfoils with complex geometry was excluded. In addition, the selected airfoil shape must be thick enough to be able to contain the wing spars.

The final group of airfoils were compared in terms of the parameters shown in table 4.3. The analysis was made using *XFLR5* software (*Xfoil Direct Analysis*), and for a Reynolds number (Re) of about 650,000. According to the results plotted in figure 4.4 and shown in table 4.3, the **NACA 6412** airfoil was chosen because despite having a lower maximum lift coefficient $C_{L_{max}}$, this airfoil would provide lower drag values while it also maintains a high lift to drag ratio.

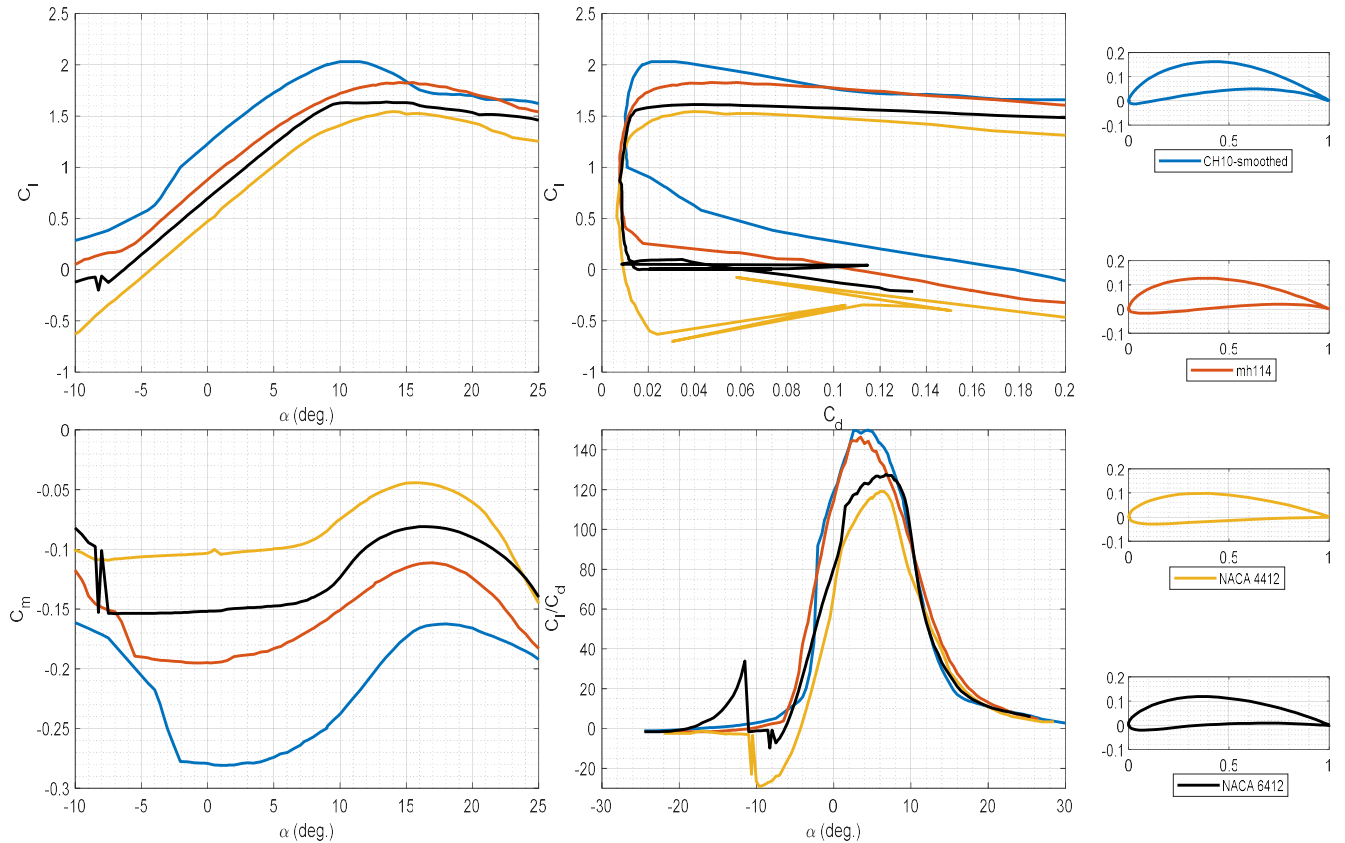


Figure 4.4: Airfoils Geometry and Performance Analysis – Plotted by MATLAB

Table 4.3: Airfoil Parameters Comparison

Parameter	CH10 – smoothed	MH114	NACA 6412	NACA 4412
Max. thickness %	12.8	13	12	12
Camber %	10.2	6.6	6	4
Max. Lift Coefficient ($C_{L_{max}}$)	2.05	1.82	1.64	1.55
Stall AOA α_{stall}	11	14.5	15	15.5
Max. Lift/Drag	150	142	125	118
AOA at Max. Lift/Drag	4	3	6.8	6.3

4.4.2 High-Lift Devices

Due to the need for a high lift coefficient during the takeoff phase to shorten the ground-roll takeoff distance, we decided to add flaps in order to increase the wing lift coefficient during takeoff and landing. Due to the nature of this year's missions' requirements, and with our design choice of designing for a high cruising speed, adding flaps is more convenient than using a cambered airfoil, this is simply because such airfoils would induce much higher drag at high speeds.

Figure 4.5 illustrates the effect of extending a flap of 30% chord length with 25° on the lift coefficient of the NACA 6412 airfoil, which is an increase in the maximum lift coefficient by about 16%.

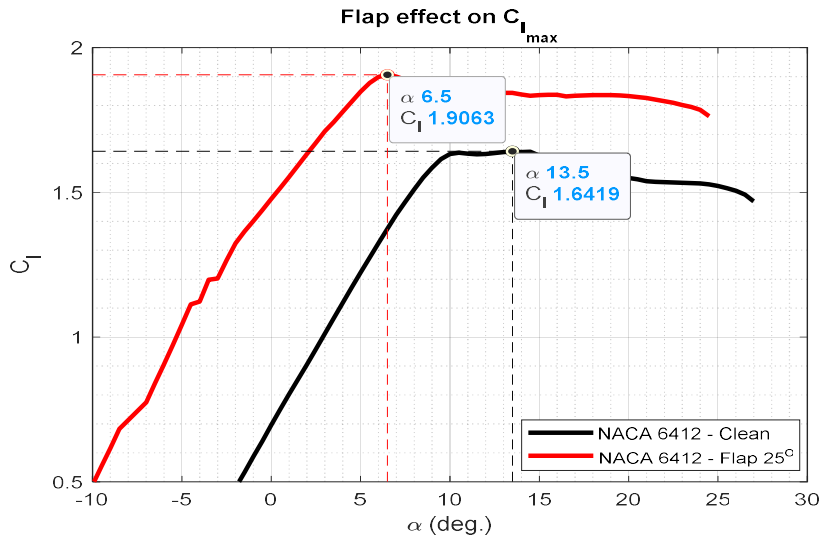


Figure 4.5: Flap Effect on NACA 6412 Lift Coefficient

4.4.3 Drag Calculation

An accurate calculation for the aircraft drag is necessary in order to predict performance and to influence improvements. The total drag is a combination of parasite drag and induced drag. In addition, drag due to the towed banner will also be present this year, which will be separately discussed.

Banner drag was calculated using semi-empirical formulae [2] and validated through wind-tunnel tests. Parasite drag was calculated based on the components' drag buildup method [3]. Induced drag was calculated for the complete aircraft using *XFLR5* software.

Banner Drag

Several research papers were investigated and studied by our aerodynamics sub-team members to stand on a proper method/formula to calculate the banner drag coefficient based on the banner geometrical and physical properties. Equations 4.10 and 4.11 represent. Furthermore, drag approximation empirical formula [2].

$$C_d = \frac{\omega}{S \cdot \rho \cdot g} * 0.39 * AR^{-1.25} + 0.012 \quad (4.10)$$

$$D(lb) = C_d \cdot A \cdot \rho \cdot V^2 \quad (4.11)$$

Where ω is the weight per unit area, A is in ft^2 , $\rho = 0.002378 \text{ slug}/ft^3$ and $g = 32.2 \text{ ft}/s^2$.

This approximation was used early on in the conceptual design phase to conduct several trade studies and sensitivity analyses, and to influence the choice of the banner size. However, moving forward into more in-detail analysis of the banner drag, wind-tunnel tests were performed on several banners having the same size but made out of different material and having different designs, these tests are detailed in section 7.2.3.

Figure 4.7 shows the measured drag force against the airspeed for three different banner lengths.

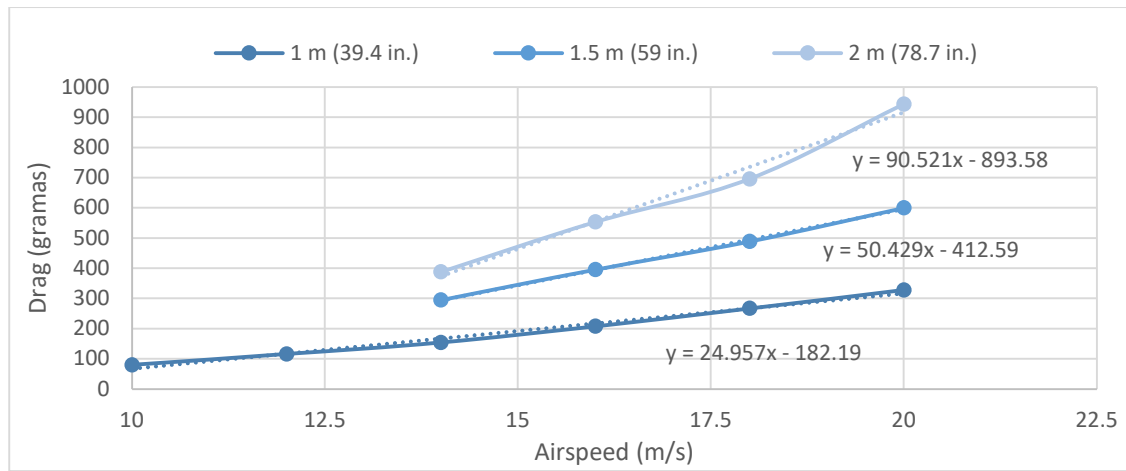


Figure 4.7 Wind-tunnel drag results against airspeed

In order to generalize these experimental data and to predict the drag of different banner lengths at various speeds, these data was fitted into a surface equation which is of second degree in airspeed (V) and first degree in banner length (L). Equation 4.12 shows the surface equation which is also plotted in figure 4.8 below.

$$\text{Banner Drag} = 1031 - 106.5 \times V - 639 \times L + 2.088 \times (V^2) + 61.47 \times (V \times L) \quad (4.8)$$

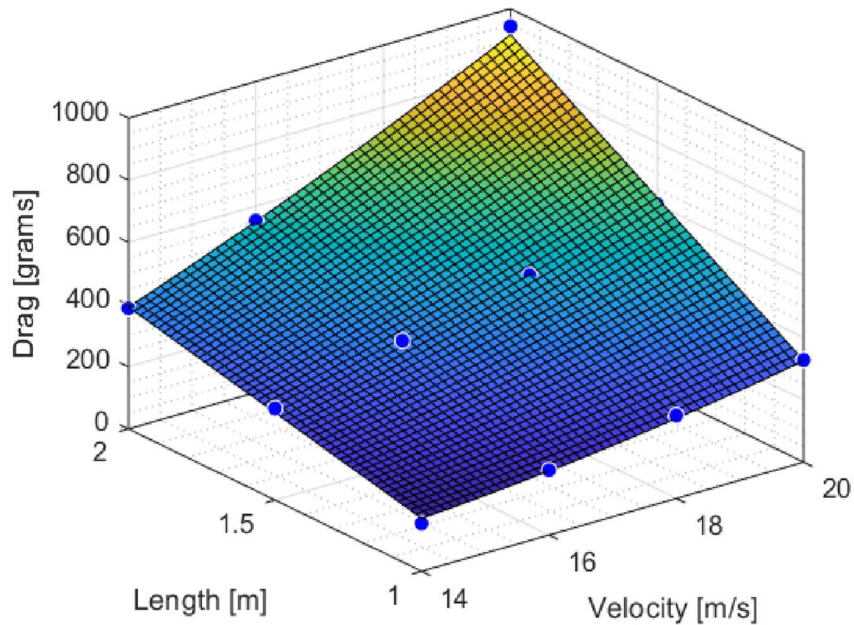


Figure 4.8: Fitted Curve of Banner Wind Tunnel Data

Based on the above results, the predicted drag of a 3 meter (118.11 inch) length banner as a function of the airspeed is given by equation 4.12 below.

$$\text{Drag} = -886 + 77.91 \times V + 2.088 \times V^2 \quad (4.12)$$

Accordingly, for a chosen cruise speed of 30 m/s (98.4 ft/s) the banner drag coefficient – referenced to the a/c wing area – can be given in equation 4.13 below.

$$C_{D_0\text{banner}} = 0.0326 \quad (4.13)$$

Parasite Drag Estimation

The parasite drag coefficient was estimated according to the component drag buildup method which is based on the estimation of flat plate skin friction coefficient (C_f) over the surfaces exposed to the airflow, and is corrected using the form factor (FF) to compensate for pressure drag due to separation and the interference factor (Q) to compensate for components' interference effect. The main formula is shown in equation 4.4, taken from Raymer's book (Aircraft Design) [3].

$$C_{D_0} = \frac{\sum(C_f * FF * Q * S_{wetc})}{S_{ref}} \quad (4.4)$$

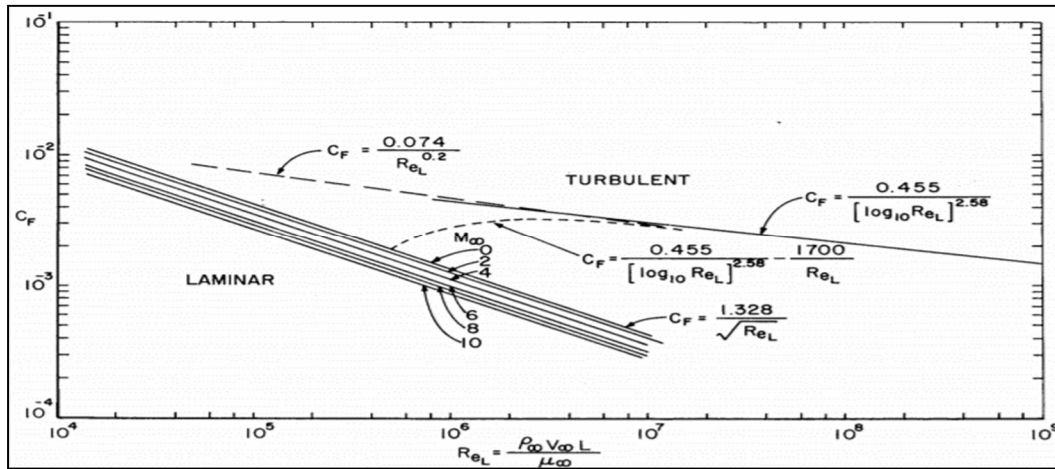


Figure 4.8: Variation of the Skin Friction Coefficient with Reynolds Number

As shown in figure 4.8, the calculation of the flat plate skin friction coefficient (C_f) depends on Reynold's number. Equations 4.5 and 4.6 are used to calculate C_f for laminar and turbulent flow respectively [3].

$$C_{f\text{laminar}} = \frac{1.328}{\sqrt{Re}} \quad (4.5)$$

$$C_{f\text{turbulent}} = \frac{0.455}{(\log_{10} R)^{2.58} * (1 + 0.144M^2)^{0.65}} \quad (4.6)$$

The form factor (FF) is calculated for the wing, horizontal tail, vertical tail, and the landing gear struts using equation 4.7, while it is calculated for the fuselage using equation 4.8.

$$FF = 1 + \frac{60}{f^3} + \frac{f}{400} \quad (4.7)$$

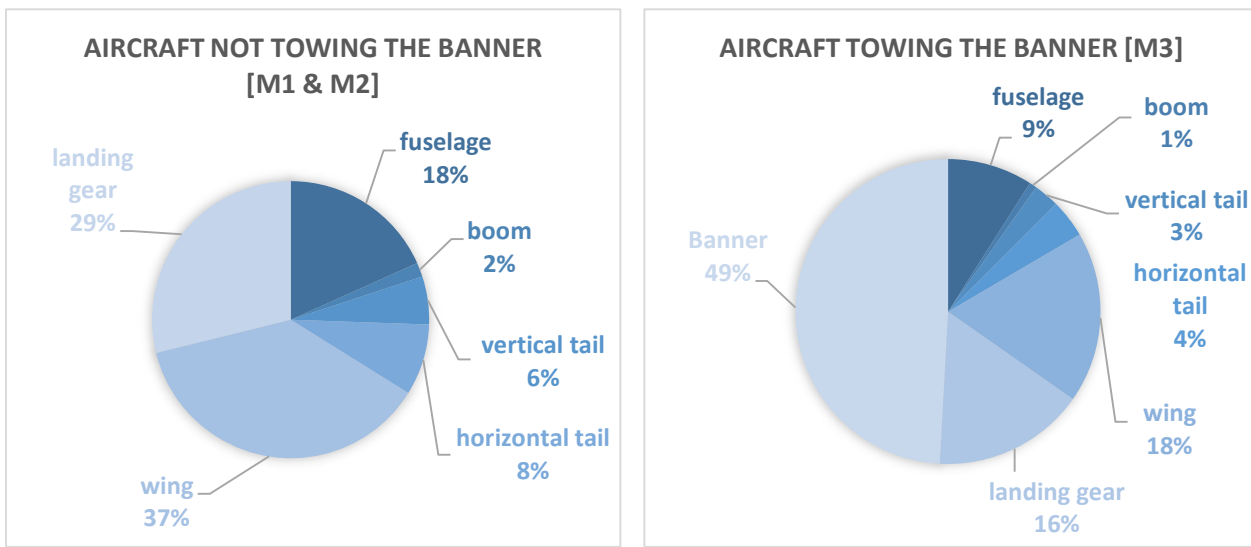
$$FF = 1 + \frac{0.6}{x/c} * \left(\frac{t}{c}\right) + 100 * \left(\frac{t}{c}\right)^4 \quad (4.8)$$

Accordingly, the parasite drag coefficient for each of the aircraft components was calculated and tabulated into table 4.4. The total parasite drag coefficient for the complete aircraft at each mission is shown in figure 4.9.

Table 4.4: Parasite Drag Coefficient Estimation for each Component

Components	Fuselage	Wing	H - Tail	V - Tail	Tail Booms	Landing Gear
C_{D_0}	0.0066	0.01357	0.00303	0.00203	0.00061	0.01050

These components' drag along with the banner drag calculated in equation 4.13. are shown in the form of a pie-chart in figure 4.9 below to represent the total parasite drag of the aircraft during each mission.



$$C_{D_0total} = 0.0363$$

$$C_{D_0total} = 0.065114$$

Figure 4.9 Parasite Drag Pie-chart

Induced Drag

Induced drag was calculated using *XFLR5* software, where we created a model for the aircraft and conducted the analysis. Results of both the parasite and induced drag was added together in order to compute the drag polar formula for the first and second flight missions (with no banner) shown in equation 4.10, while the drag polar formula for the aircraft towing the banner is shown in equation 4.10. Both equations are plotted into figure 4.7 below.

$$\text{Clean A/C: } C_D = 0.0824 - 0.11525 \times (C_L) + 0.1441 \times (C_L)^2 \quad (4.9)$$

$$\text{A/C Towing the Banner: } C_D = 0.111214 - 0.11525 \times (C_L) + 0.1441 \times (C_L)^2 \quad (4.10)$$

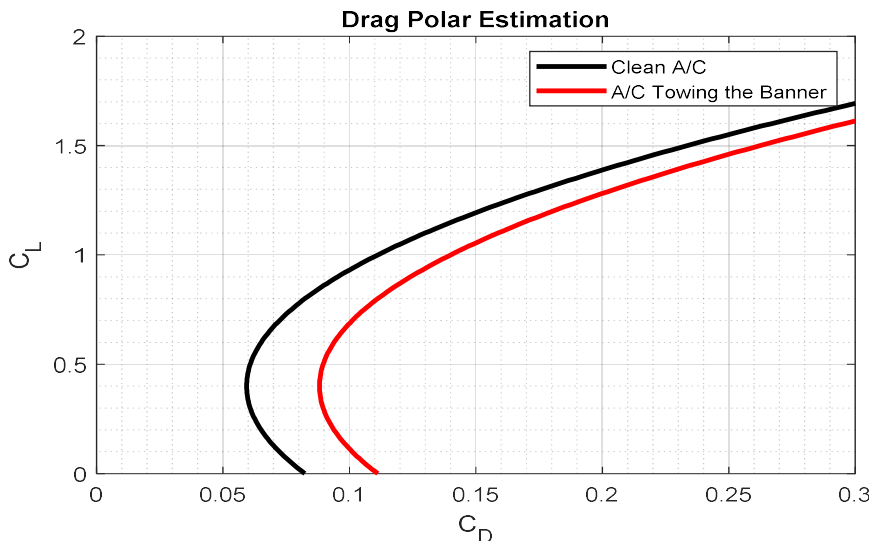


Figure 4.10: Drag Polar Estimation

CFD Analysis

Fuselage Drag

CFD analysis was conducted on the three fuselage designs mentioned in section 3.3.1, total drag and lift were calculated and compared. Although the blended body fuselage produced more lift at the takeoff, the produced drag was much bigger compared to the other configuration. Consequently, it was decided to use the round edged fuselage as it minimizes the drag and maintain the needed lift during take-off by adding high lift devices instead of the blended body fuselage. Figure 4.8 shows the skin friction distribution on the different fuselage configuration during mission three.

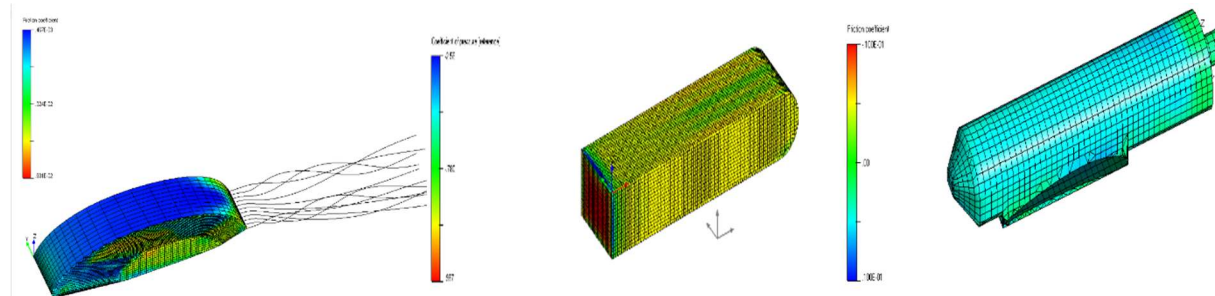


Figure 4.11: Fuselage Skin Friction Distribution

Aircraft Drag

In order to verify the drag calculated using the build up drag method, FlightStream software was used to calculate the drag of each component in mission 1, 2 and 3. The results were compared to those obtained using build up drag method and tabulated in table 4.4 below.

Table 4.4: Components Drag Results Comparison

Components	Fuselage	Wing	H - Tail	V - Tail	Tail Booms	Landing Gear
C_{D_0} (Build up drag)	0.0066	0.01357	0.00303	0.00203	0.00061	0.01050
C_{D_0} (Flightstream)	0.0063	0.0137	0.0029	0.0019	0.0007	0.0105

The results obtained were found to be very similar to those estimated using the buildup drag method. Figure 4.11 shows the pressure contour on the aircraft for 0 angle of attack and a velocity of 160 ft/s.

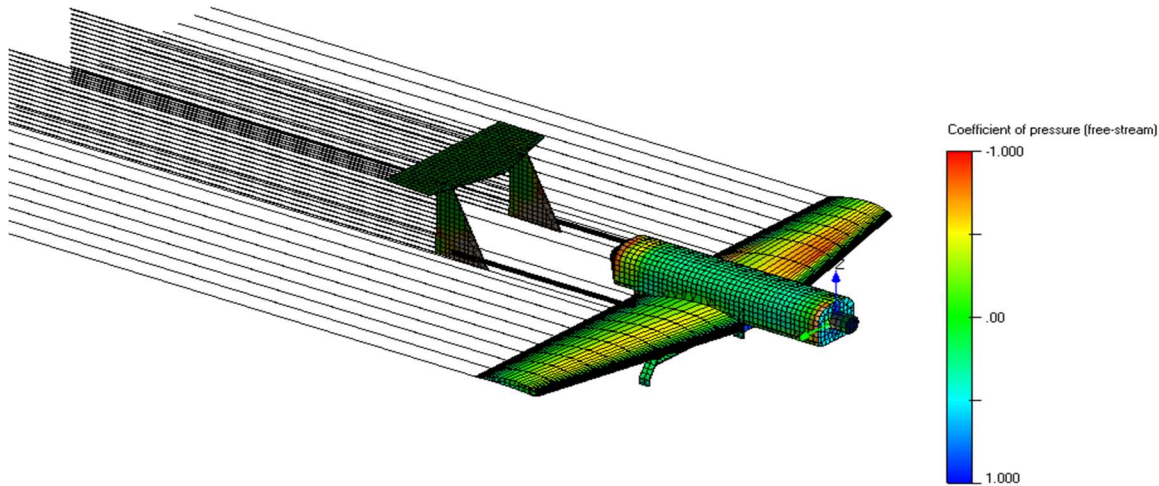


Figure 4.11 Pressure contour on the aircraft

4.5 Stability and Control

4.5.1 Longitudinal Static Stability

Tail Sizing

Tail sizing is done to provide the longitudinal stability of the aircraft through ensuring a positive C_{m_0} and a negative C_{m_α} (slope). Following the tail sizing methodology from [4], both the horizontal and vertical tail volume expressions - in equations 4.10 and 4.11 respectively - were equated to their recommended values.

$$V_h = \frac{S_h * l_h}{S * MAC} = 0.56 \quad (4.10)$$

$$V_v = \frac{S_v * L_v}{S * b} = 0.09 \quad (4.11)$$

This yields the relation between each tail area and the tail arm, which is plotted in figures 4.11 and 4.13. The desired value for each tail arm decides the tail area. Dimensions of each surface is illustrated in figures 4.12 and 4.14.

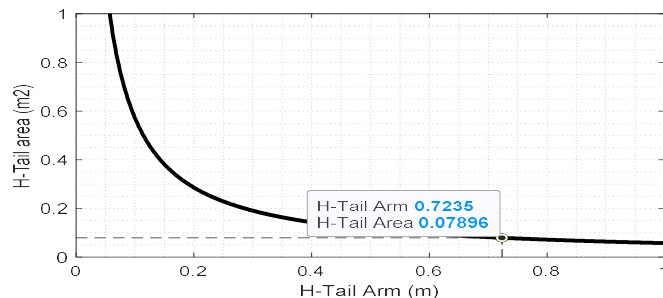


Figure 4.11 Horizontal Tail-arm versus its Planform Area

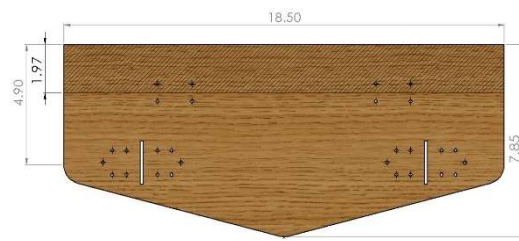


Figure 4.12 Horizontal Tail Geometry

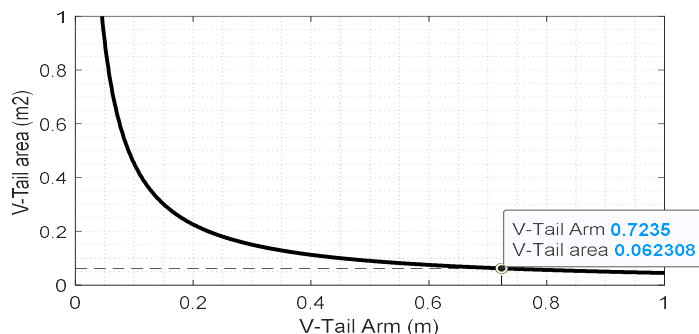


Figure 4.13 Vertical Tail-arm versus its Planform Area

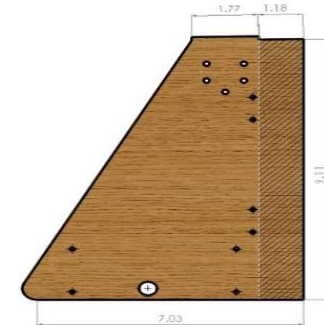


Figure 4.14 Vertical Tail Geometry

Static Margin and CG Location

The static margin, which is the distance between the neutral point and the center of gravity, is given by equation 4.16 below [4]. A well-behaved aircraft typically has a static margin in the range of 5% to 15% as this is suggested to provide good stability characteristics [5].

$$SM = \frac{X_{NP} - X_{CG}}{MAC} \quad (4.16)$$

$$\frac{X_{NP}}{MAC} \cong \frac{1}{4} + \frac{1 + 2/AR}{1 + 2/AR_h} \left(1 - \frac{4}{AR + 2} \right) * V_h \quad (4.17)$$

The neutral point for the aircraft was either calculated from *XFLR5* software, or via equation 4.17 [4]. Once the neutral point is calculated for each mission, the static margin corresponding to the center of gravity location is calculated for that mission, documented below in table 4.5.

Table 4.5: Missions' static margin

Missions	X_{CG} (inches)	Static Margin
M1	6.89	11.96%
M2	7.09	10.18%
M3	6.97	11.25%

As shown in figure 4.15, the two requirements for static stability are satisfied; where the slope ($C_{m\alpha}$) is negative and also the value of ($C_{m\alpha}$) is positive. Although, for mission 3 it may be required to apply small elevator deflection for a better trimming angle.

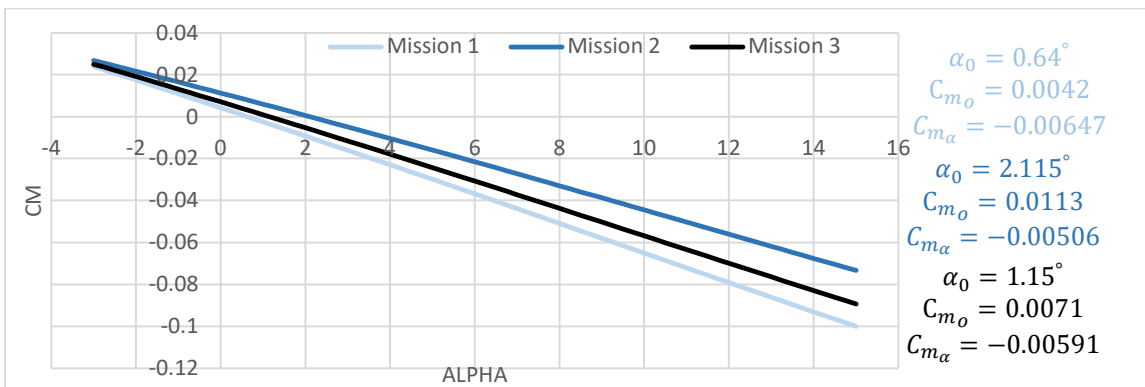


Figure 4.15: C_m vs. α Curves

Dynamic Stability

Using *XFLR5* software, the aircraft's modes of motion in each mission was plotted into figure 4.16, namely they are Phugoid (Long Period) and Short Period for longitudinal modes, and Spiral, Roll and Dutch Roll for lateral modes. The aircraft is stable in all modes but has an unstable spiral mode as it lies on the right half plane. However, the spiral mode has a minimum time to double amplitude of 8.5 seconds which is enough for the pilot to safely react out of it. Furthermore, figure 4.167 shows the time response for both the longitudinal and the lateral modes.

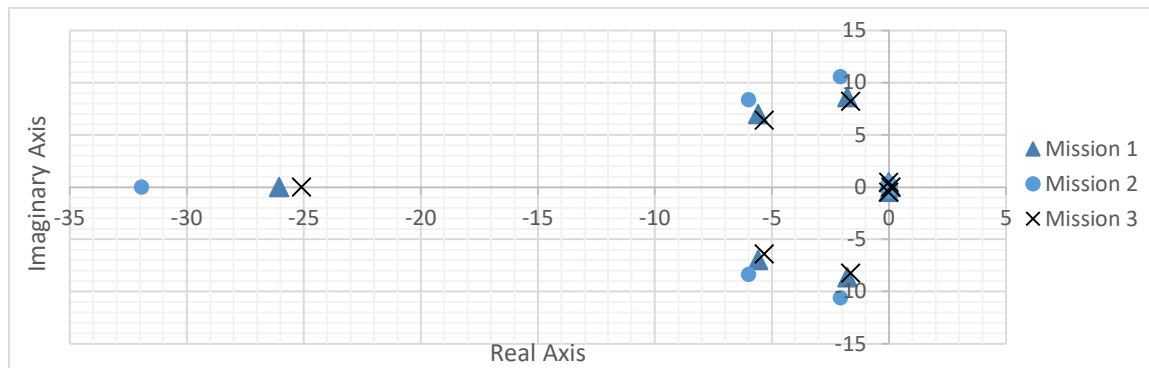


Figure 4.16: Pole-Zero Diagram from *XFLR5* Software – Plotted by Excel

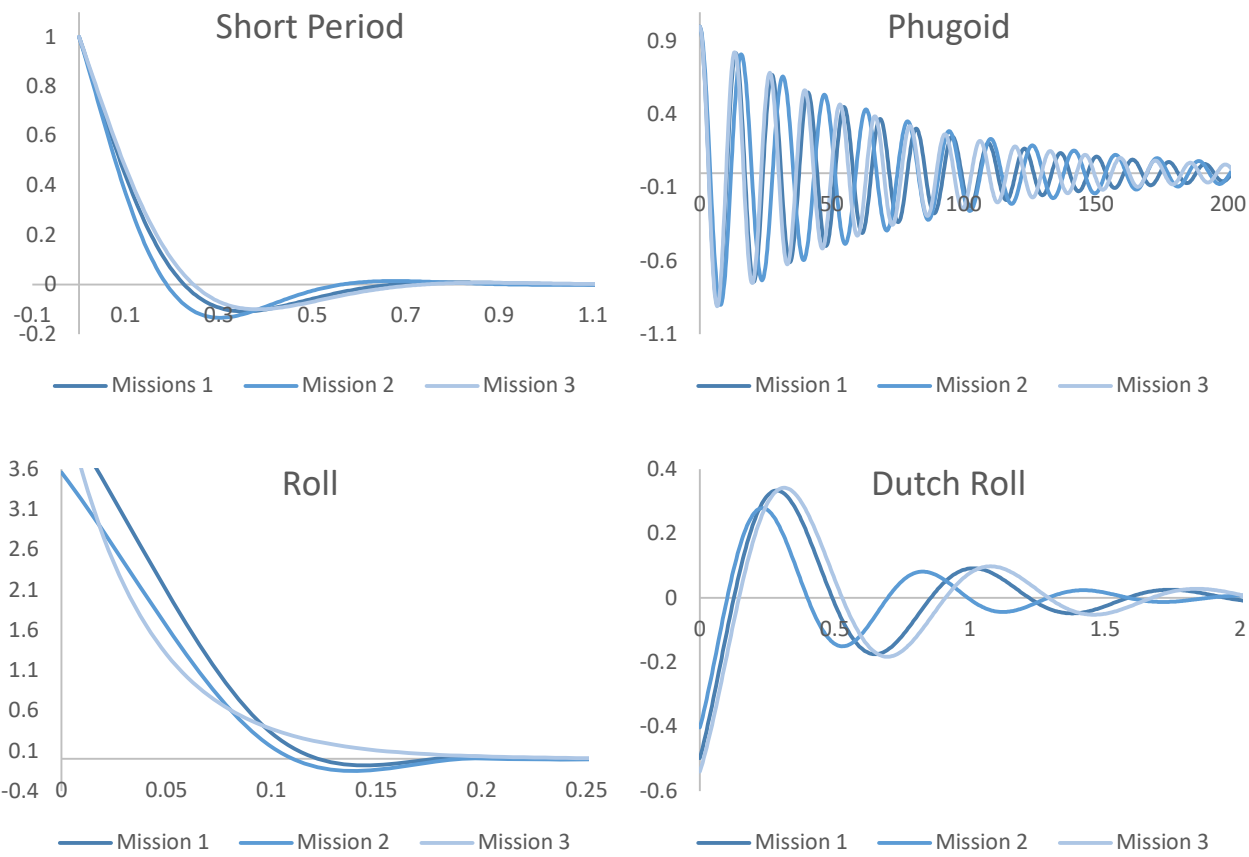


Figure 4.17: Time Response Plots

The dynamic stability modes damping ratio (ζ), undamped natural frequency (ω_n), damped frequency (ω_d) and time to double amplitude (t_2) for unstable poles or time for half amplitude ($t_{1/2}$) for stable poles were tabulated into table 4.7 below. All dynamic stability characteristics lies within the acceptable range mentioned in [5].

Table 4.6: Dynamic Stability Characteristics

Mode	Mission 1				Mission 2				Mission 3			
	ζ	ω_n (Hz)	ω_d (Hz)	t_2 or $t_{1/2}$ (sec.)	ζ	ω_n (Hz)	ω_d (Hz)	t_2 or $t_{1/2}$ (sec.)	ζ	ω_n (Hz)	ω_d (Hz)	t_2 or $t_{1/2}$ (sec.)
Short Period	0.625	1.112	1.424	-	0.58	1.334	1.64	-	0.64	1.02	1.327	-
Phugoid	0.032	0.073	0.073	-	0.033	0.064	0.064	-	0.03	0.072	0.072	-
Spiral	-	-	-	9.628	-	-	-	11.82	-	-	-	8.506
Roll	-	-	-	0.027	-	-	-	0.031	-	-	-	0.028
Dutch Roll	0.201	1.374	1.402	-	0.192	1.685	1.717	-	0.195	1.31	1.336	-

Aileron Sizing

The roll authority and the roll damping for the aileron are given by equations 4.12 and 4.13 respectively [1].

$$C_{l_{\delta_a}} = \frac{c_{l_{\delta_a}} C_R}{Sb} \left[(b_2^2 - b_1^2) + \frac{4(\lambda - 1)}{3b} (b_2^3 - b_1^3) \right] \quad (4.12)$$

$$C_{l_p} = -\frac{(C_{l_{\alpha}} + C_{d0}) C_R b}{24S} [1 + 3\lambda] \quad (4.13)$$

Solving the previous two equations for a desired roll authority ($C_{l_{\delta_a}}$) of $0.012 / \text{deg}$ and a desired roll damping of $-0.037 / \text{deg}$ and using the parameters of the wing yields the required geometry for the ailerons to be of a 0.824 ft. span and a 3.455 in. mean chord, and is located between $b_1 = 1.39 \text{ ft.}$ and $b_2 = 2.214 \text{ ft.}$ span-wise, as shown in figure 4.18.

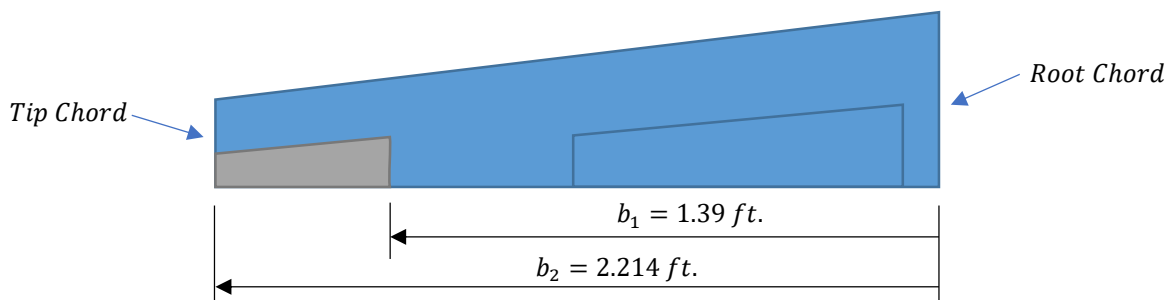


Figure 4.18: Aileron Geometry

4.6 Mission Performance Estimations

The mission model discussed earlier in section 4.3 was used to predict the performance of the chosen preliminary design in each of the three missions, and consequently, the score of each mission was calculated. Results are tabulated into table 4.7 below.

Table 4.7: Calculated Missions' Performance

Parameter	Mission 1	Mission 2	Mission 3
$C_{L_{Max}}$	1.6	1.6	1.6
$C_{L_{Cruise}}$	0.437	0.2	0.488
C_{D_0}	0.055	0.055	0.06
$(L/D)_{max}$	16.95	16.95	14
$(L/D)_{cruise}$	16.2	11.86	13.84
Take-off distance (ft.)	18	29.53	18
Rate of climb (ft/s)	19.7	11.5	16.4
V_{stall} (ft/s)	47.6	52.5	49.2
V_{cruise} (ft/s)	82	147.6	82
V_{turn} (ft/s)	65.6	60.7	55.8
Turning Radius (ft)	19.7	29.5	29.5
Wing Loading [W/S] (psf)	3.3	5	3.5
Gross weight (lbs.)	13.2	19.8	13.9
Lap Time (sec.)	30	23	32

5.0 Detail Design

5.1 Dimensional Parameters

This subsection details the final aircraft main dimensions and the main specifications of our propulsion system. Which came out as the results of an iterative process of tests and enhancements.

Table 5.1 Dimensional Parameters of the Final Aircraft

Wing		Fuselage		Motor	
Airfoil	<i>NACA 6412</i>	Length	25.6 in	Model	<i>Scorpion HKII – 4225</i>
MAC	11.09 in	Max. Width	5.9 in	KV	550
Span	5 ft.	Max. Height	4.9 in	I_o	1.77 A
Aspect Ratio	4.91			Power	5770 Watt
Area	3.99 ft ²			Total Weight	0.89 lbs
Horizontal Tail		Elevator		Batteries	
Airfoil	<i>Flat Plate</i>	Span	18.11 in	Type	<i>Lipo</i>
MAC	6.76 in	Chord	1.97 in	Capacity	2250
Area	8.6 ft ²			No. of Cells	24
Span	18.5 in			I_{max}	225 A
Incidence angle	-1°			Total Weight	3.3 lbs
Vertical Tail		Rudder		Main Landing Gear	
Airfoil	<i>Flat Plate</i>	Span	9.84 in	Width	15.74 in
MAC	5.85 in	Chord	3.45 in	Height	8.5 in
Area	0.69 ft ²				
Span	18.11 in				
Ground AoA					
12°					

5.2 Structural Characteristics and Capabilities

5.2.1 Layout and Design

Flying on a relatively high speed, this year our structural layout was designed in a way that all loads are transferred to the major load-withstanding components, including the massive aerodynamic loads due to high cruising speeds beside the dynamic load caused by the fluttering banner in mission 3. The main structural component is a frame of spars that bear the transferred load from all of the aircraft. This frame structure consists of the main wing spars connected to both the booms that hold the empennage, and the main fuselage spars. This way all the loads on the wing are safely transferred to the main wing spars, the loads due to banner flutter are transferred to the fuselage then to the fuselage spars. The challenging part was designing the attachment points and joints to withstand this load transfer.

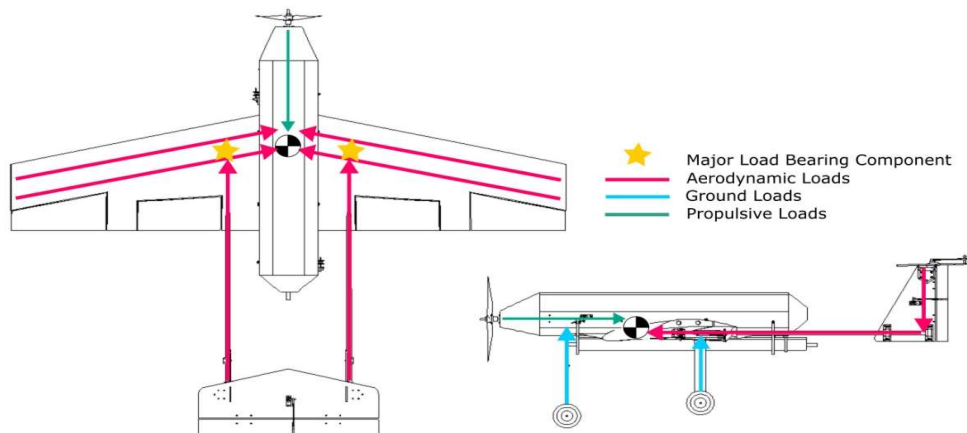


Figure 5.1: Load Paths of Major Forces

5.2.2 Flight Envelope

Using the expected maximum load cases, the aircraft was designed to withstand the load of a 15g in missions 1 and 3. As for the charter flight mission the aircraft would safely withstand a load of 10g. After analyzing the flight missions to determine the operational flight envelope for our aircraft, the resulting V-n diagram is shown in figure 5.2.

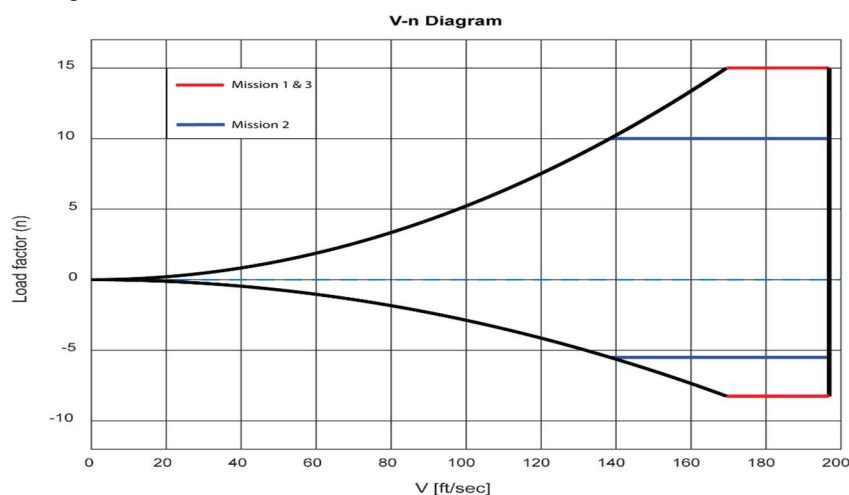


Figure 5.2: V-n Diagram

5.3 Sub-systems design and integration

In order to meet the required performance parameters each part of the aircraft should be compatible with the other parts, stiff enough to carry the large structural loads, reliable and efficient besides the manufacturing simplicity. Therefore, each separate part had passed an optimization process to achieve the required performance taking into considerations the integration among all sub-systems and their functions to get smooth performance.

5.3.1 Wing structure

The wing is mainly made of blue foam and supported by two carbon fiber spars. The spars are fitted into two paxolin joints with the tail booms, they are carved into the lower side of the blue foam, then this lower side is covered by MonoKote layer to retain the airfoil shape. This design allows for a very lightweight structure yet can endure significant loads.

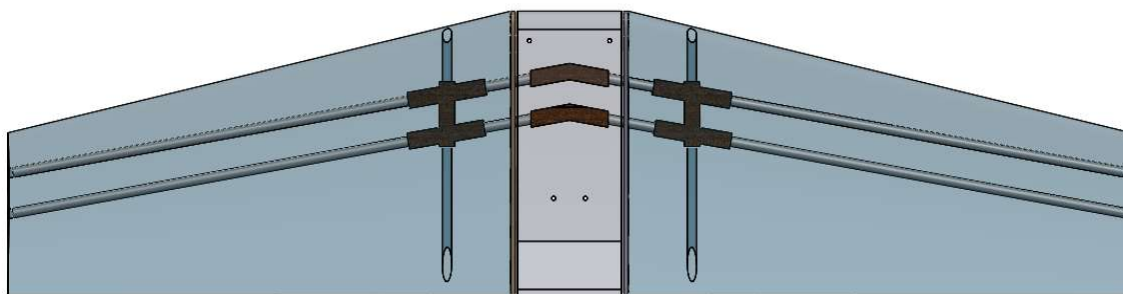


Figure 5.3: Wing Structure

Connectors

There are two main wing spars connectors responsible for connecting the two wing halves in addition to giving it the required swept and dihedral angles.

Spars

Therefore, we chose the wing spars to be carbon fiber with outer diameter 0.47 in and 0.63 in for the front and rear wing spars respectively. Also, the booms were chosen to be carbon fiber with 0.63 in outer diameter.

5.3.2 Fuselage design

The fuselage is designed to support severe flight loads and landing impact loads so our foam boards technologies were not going to withstand these loads so plywood was chosen as the fuselage material. The fuselage mainly consists of two side spars with a ground plate between them, the cross-sectional shape was given using 5 bulkheads mounted to the ground plate and supported by the fuselage wooden spars from the side. This design increased the rigidity of the fuselage against torsion loads and the dynamic loads encountered due to fluttering banner.



Figure 5.5: Fuselage Interior Structure

Wing - Fuselage Fixation

As mentioned in the design layout in section 5.2.1, the main load bearing components are the spars frame structure and the joint connecting them. So, both the wing and the fuselage are attached to this interior structure as the wing spars passes through a spar connector located in the fuselage. The low wing configuration adds more rigidity to the structure.

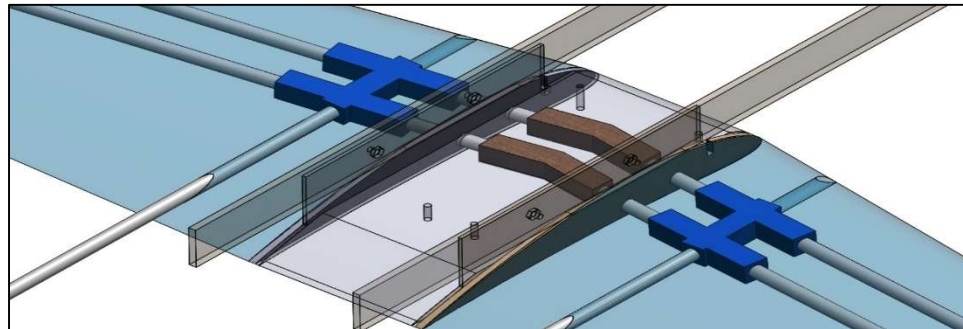


Figure 5.6: Wing Fuselage Fixation

Banner Deploying and Releasing Mechanism

- Deploying Mechanism**

Figure 5.7 shows the banner deploying mechanism consists of two servos each of which is attached to a pin holding a rubber band between two metal rings. These two servos are located on the side spar of the fuselage. When the servomotor arm moves, it pushes the pin out of the first ring releasing the rubber band and thus deploying the banner. The two servos are on the same channel on the transmitter to avoid jamming during the deployment.

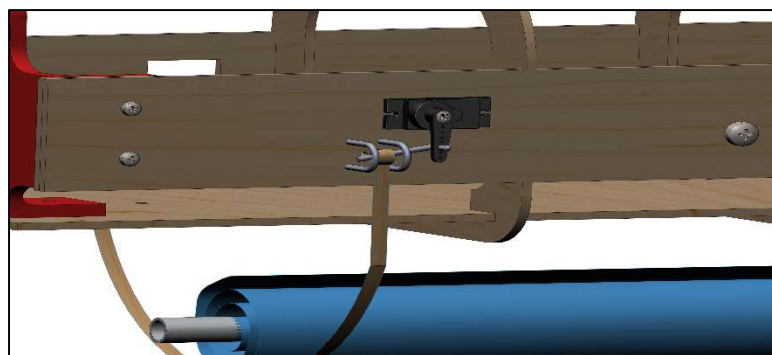


Figure 5.7: Banner Deployment Mechanism

- **Releasing Mechanism**

The releasing mechanism shown in figure 5.8 is similar to the deployment mechanism as the end of the banner towing line is a ring that is held with a rod between two supports. These supports are located on the plate underneath the fuselage, this way the load of the fluttering banner is assured to be transferred directly to the main spar of the fuselage thus the main load bearing interior structure. In addition, these supports differ from the rings used in the deployment mechanism so that they can withstand the dynamic load, and hence they are made of larger metallic stronger having larger cross-sectional area.

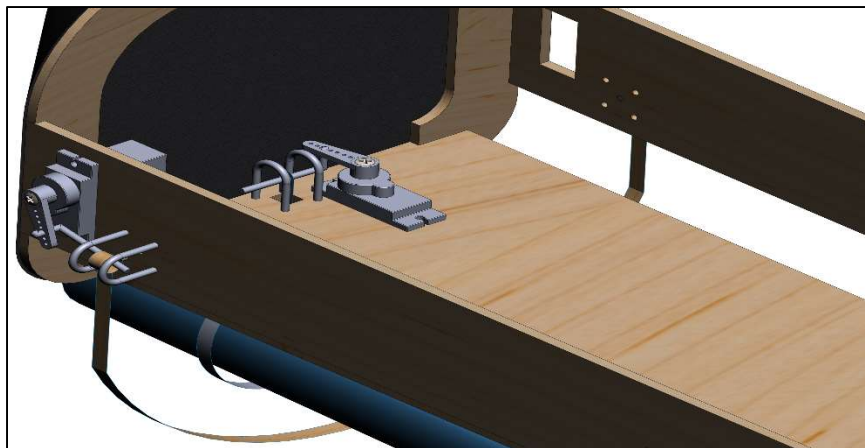


Figure 5.8: Banner Releasing Mechanism

Passengers and luggage compartments

The passenger's compartment is a simple box with a mid-plate having holes equal to the number of passengers and having the same diameter to hold them in place. Additionally, the box cover has engravers that match the upper curve of the passenger head to prevent any movement during flight.

The luggage compartment consists of 7 columns each carry three luggage. Each column has a spring connected to its inner bottom from one end and to a plate on which the luggage is inserted from the other end. The role of the spring is to push each luggage up easily once the prior one was removed. The passengers and luggage compartments are both shown in figure 5.9.

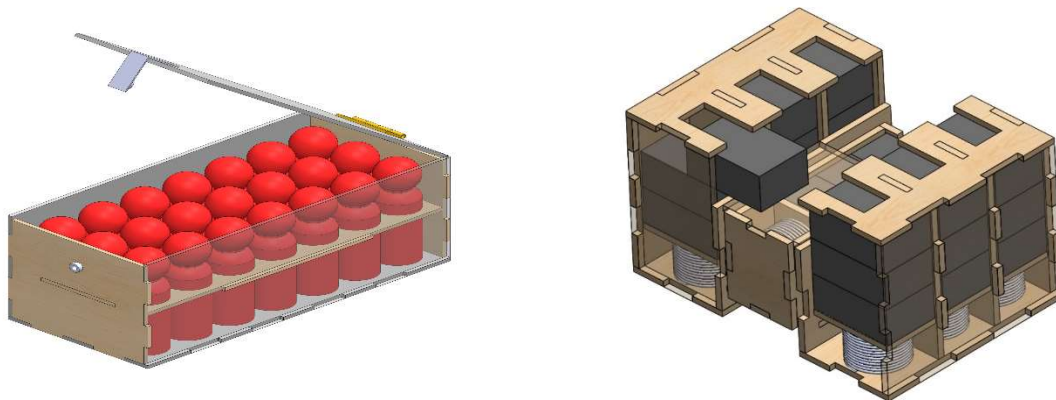


Figure 5.9: Passengers and luggage Compartment

5.3.3 Landing gear

Tricycle configuration was selected to be our aircraft landing gear design. This configuration outperforms the other undercarriage configurations since it guarantees the largest ground clearance in order to avoid any contact between the banner mechanism and ground as well as preventing our aircraft large propeller from touching the ground. Also, this landing gear configuration has the most efficient handling capabilities comparing with the other configurations and this will facilitate the steering control in take-off phase.

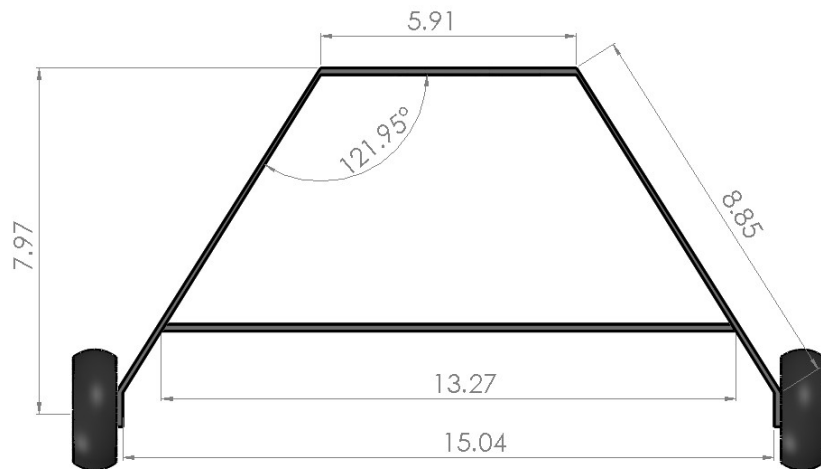


Figure 5.10: Main Landing Gear

5.3.4 Empennage

The empennage construction mainly depends on using 1.2 in plywood to enhance its stiffness. The connection between horizontal and vertical tail will be 3D printed parts with stated specifications in order to bear the acting forces on tail assembly connections. Aluminum hinges will be used as elevator and rudder hinges to ensure smooth and reliable work. The connection between empennage and fuselage are two 0.63 in carbon fiber circular rods fixed to the empennage using 3D printed joints which had been tested for withstanding stresses created by tail assembly. The complete empennage assembly is shown in figure 5.11 below.

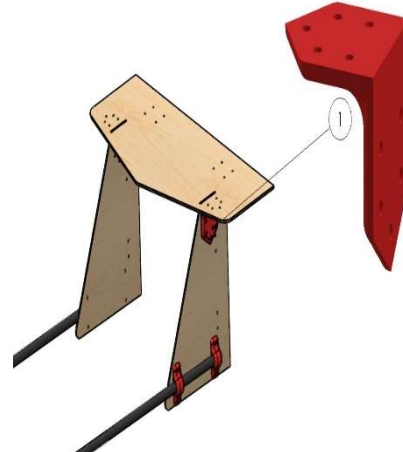


Figure 5.11: Tail Assembly and connector

5.3.5 Receiver and Transmitter Selection

The team choice was Spectrum AR9020 to be the aircraft receiver and a Spectrum DX9 as a transmitter both will be used to control our aircraft in its ground and flight missions. So, at least the aircraft needs a receiver with 9 channels to control all the control surfaces and the banner mechanism. A separate NiMH batteries pack were used to power the receiver.

5.3.6 Servo Selection

Two main types of servos shown in figure 5.12 are used in the aircraft; they are categorized according to the loads each must endure after analyzing the hinge moments and the required actuating torques. First, Futaba S3010 servos that are responsible for actuating the control surfaces these servos are similar to those of the banner deploying mechanism for these applications we used FS5109M servos. As for the relatively heavy-duty servo used in the releasing mechanism a bigger metal gear servo is used, in order to withstand the dynamic load applied to the rod holding the fluttering banner especially during turnings. This metal gear servo with the rod and supports are tested in a wind tunnel test at the expected cruising speed of 160 ft/s.



Figure 5.12: Selected Servos

5.3.7 Propulsion System

The top performing propulsion systems that were chosen using eCalc software in section 4.2.2, were set up for testing. In order to calculate the dynamic thrust, the rpm of the various combinations was found using eCalc to estimate the dynamic thrust from the APC propeller performance database [6].

The results were then verified using two methods: The first method was depending on the set of experimental data found on UIUC propeller data site [7]. And the second method was conducting tests for the actual thrust using a wind tunnel which will be detailed in section 7.3.1.

MaxAmps 2250 custom made LiPo 12 cell battery packs were carefully chosen for our propulsion system as they provide power, speed and endurance required for completing the flight missions within the required flight window.

According to the preformed tests, out of all considered motors the Scorpion HKII-4225 motor along with its electronic speed controller were chosen as they provide sufficient thrust for take-off and cruising at 160 ft/s while having the least overall system weight. A total of 2 LiPo battery packs connected in parallel having 12 cells each and a 12x8 APC electric propeller will be used for missions 1 and 2, while two LiPo battery packs of 9 cells having higher capacity will be used in mission 3 for more endurance.

In order to verify that the final chosen propulsion system meets all requirements, thrust versus velocity curve shown in figure 5.13 was plotted. Assuming that the drag is equal to the thrust required, the thrust

curve was found by calculating the drag on the aircraft in flight missions for a large range of cruising speeds. While the dynamic thrust data collected during the wind tunnel testing where curve fitted to plot the thrust available curves at 60% and full throttle. The point where the thrust required and available meets is the optimum performance point.

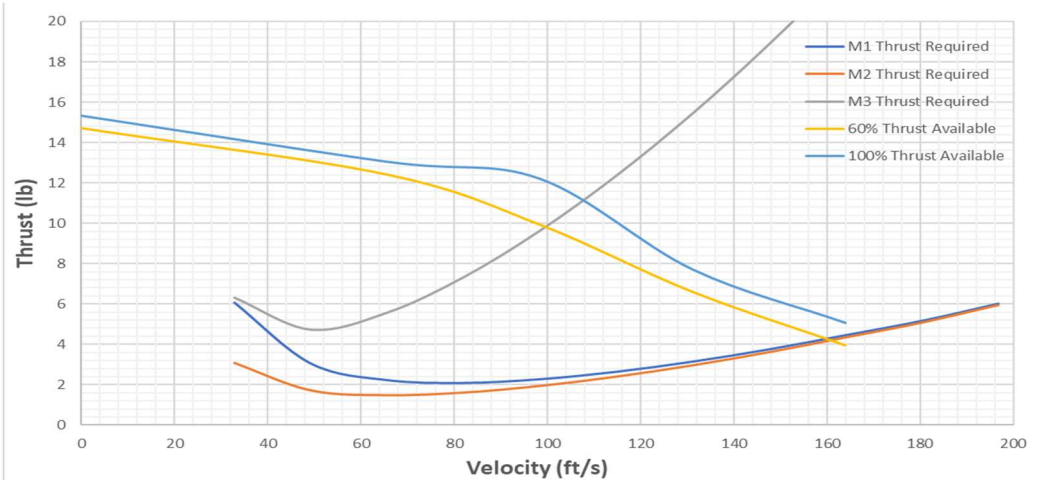


Figure 5.13: Thrust Vs Velocity Curve

The different propulsion system combinations that will be used in each flight mission are shown in table (5.2). The estimated endurance for mission one is 4 minutes. While it was predicted that the batteries will last about 2 minutes in mission 2 which will allow for completing 3 laps while flying at 160 ft/s and carrying 18 passengers. For mission 3 the batteries will last between 6 and 7 minutes.

Table 5.2: Propulsion System for each Mission

Components	Missions 1 & 2	Mission 3
Motor	Scorpion HKII-4225-550KV	
Propeller	APC 12x8E	APC 12x6E
ESC	Scorpion Tribunus 12-130A	
Battery (series x parallel)	2250mAh LiPo (12x2)	3000mAh LiPo (9x2)
Receiver	Spectrum AR9020 9-Channel	
Transmitter	Spectrum DX9	

5.4 Weight and balance

Specification mass and C.G location for each aircraft component is a priority in order to ensure the aircraft static stability in different axes. Table 5.4 shows the different aircraft components C.G location and the whole aircraft C.G location. After determination the properties of all used materials and each component dimensions we used SolidWorks software to analyze these data and determine the location of C.G. The reference axes from which the dimensions were measured along with the estimated CG position for each mission are shown in figure 5.14. However, those numbers may change due to manufacturing inaccuracies. Such variations are compensated by relocation of the electrical component.

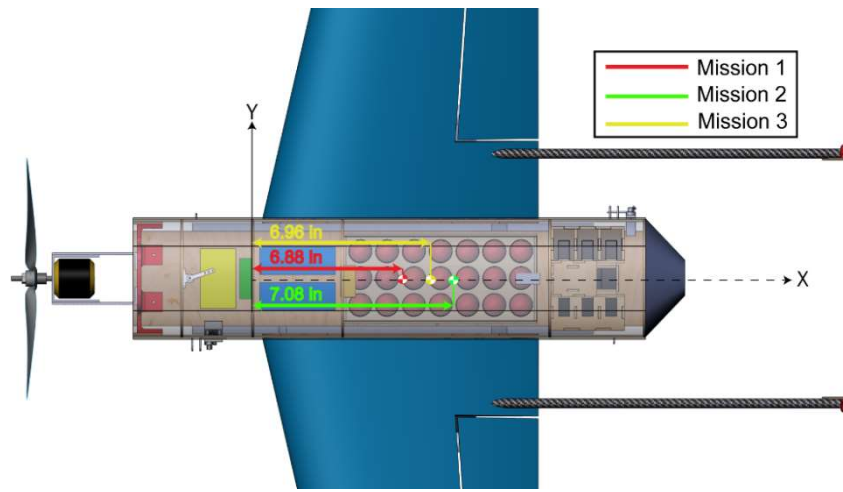


Figure 5.14: Aircraft CG Location at each Mission

Table 5.3: Weight and Balance Table

Empty weight			
Components	Mass (lbs)	CG (X-axis) (in)	CG (Z-axis) (in)
Fuselage	1.55	5.62	2.24
Wing	1.44	6.18	0.87
Motor	1.23	-9.12	2.29
Propeller	0.01	-11.6	2.17
Boom	0.06	18.71	0.65
Empennage	0.94	33.56	6.45
Main Gear	0.61	10.07	-6.47
Nose Gear	0.23	-3.74	-5.93
Passengers compartment	0.30	8.14	3.08
Luggage compartment	0.41	16.16	2.40
Total empty weight	7.43	7.14	1.49
Mission 1			
Main battery	3.31	6.58	3.16
Receiver battery	0.1	-0.85	2.03
Total aircraft	11.26	6.88	2
Mission 2			
Main battery	3.31	1.75	2.87
Receiver battery	0.1	-0.85	2.03
Passengers	5.28	8.88	2.82
Luggage	0.85	16.28	2.93
Total aircraft	17	7.08	2.25
Mission 3			
Main battery	3.31	7.5	3.16
Receiver battery	0.1	-0.85	2.03
Banner (In-Flight)	0.13	55	-0.74
Total aircraft	11.39	6.96	2

5.5 Flight and mission performance

5.5.1 Flight performance

Table 5.5 includes the expected performance for the final aircraft in each mission and key aspects like the take-off distance, stall speed and turning performance.

Table 5.5: Performance Estimations of the Aircraft in Each Mission

Performance parameter	Mission 1	Mission 2	Mission 3
$C_{l_{Max}}$	1.6	1.6	1.6
$C_{l_{Cruise}}$	0.437	0.2	0.488
C_{D_0}	0.055	0.055	0.06
$(L/D)_{max}$	16.95	16.95	14
$(L/D)_{cruise}$	16.2	11.86	13.84
Take-off distance [ft.]	18	29.53	18
Rate of climb (ft/s)	19.7	11.5	16.4
V_{Stall} [ft/s]	47.6	52.5	49.2
V_{cruise} [ft/s]	82	147.6	82
V_{turn} [ft/s]	65.6	60.7	55.8
Turning radius [ft.]	19.7	29.5	29.5
W/S [psf]	3.3	5	3.5
Gross weight [lb.]	13.2	19.8	13.9
Lap time [sec.]	30	23	32

5.5.2 Mission performance

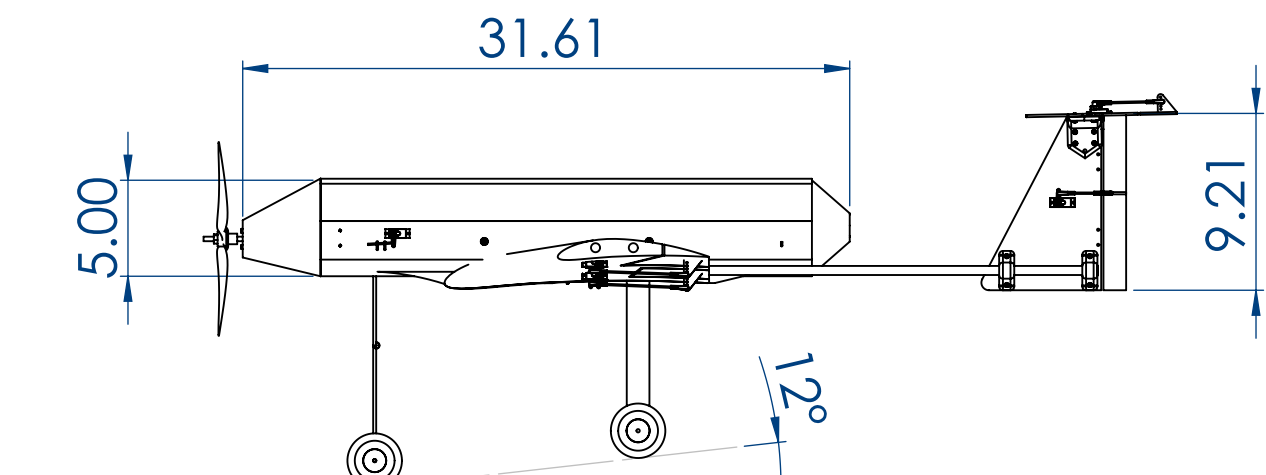
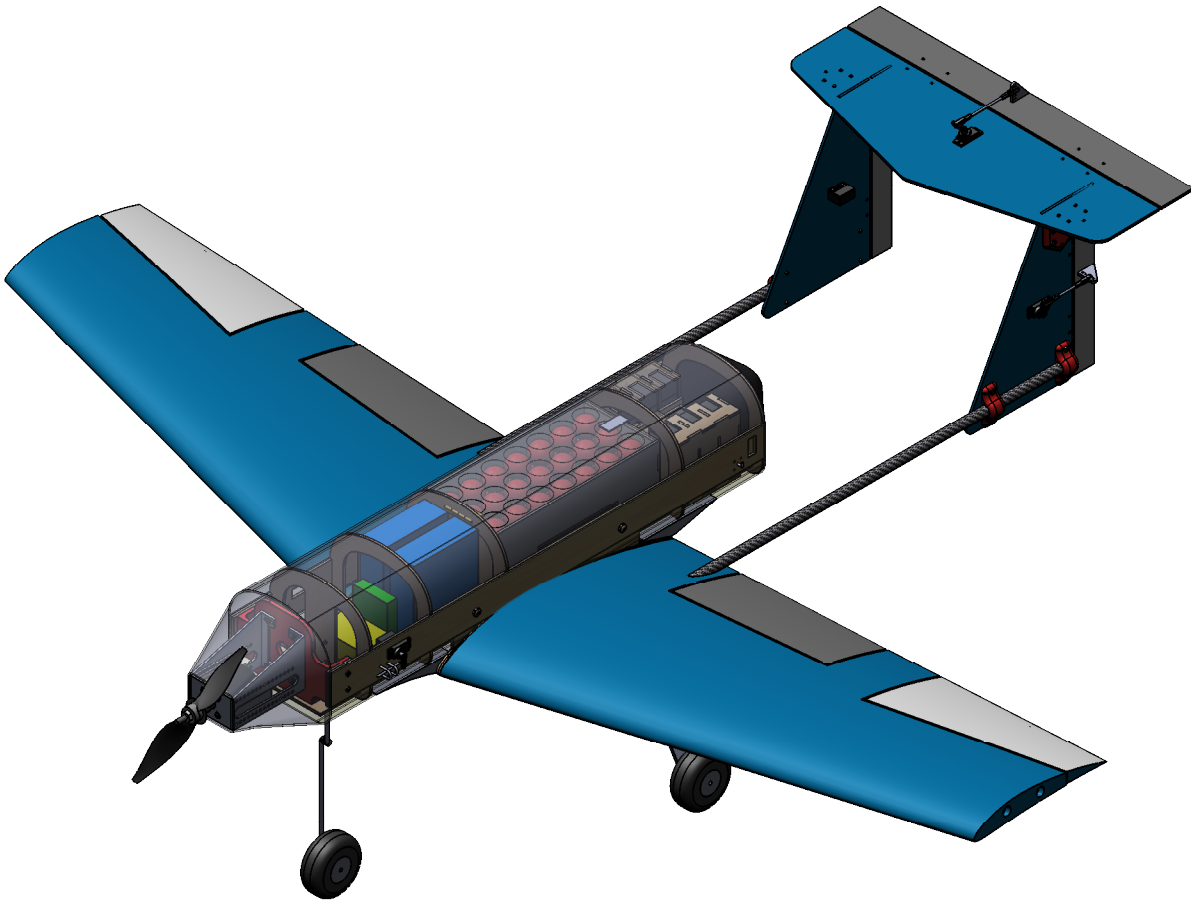
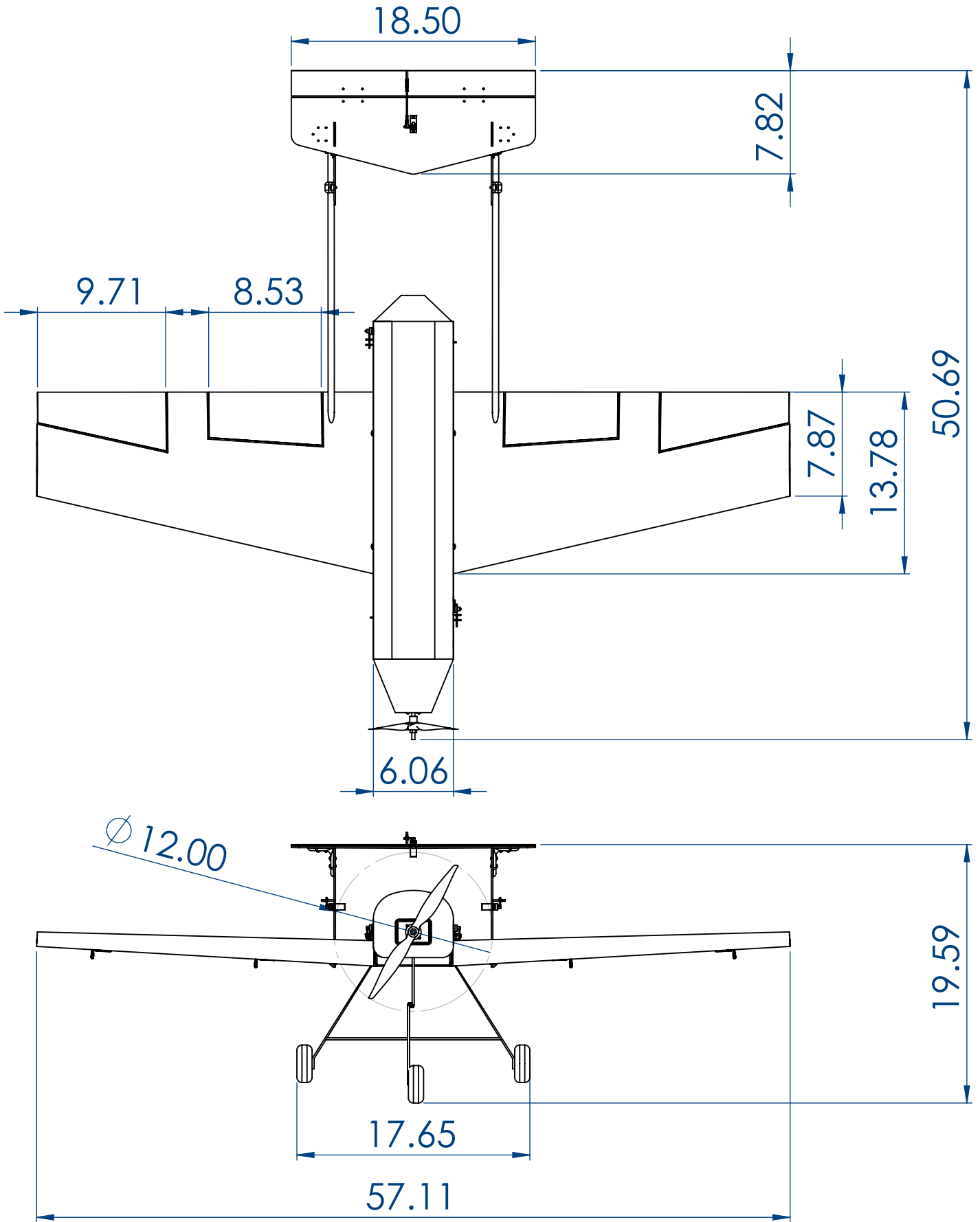
Based on the performance parameters estimation that was mentioned above as well as the mission modeling and the sensitivity analysis, the following missions' scoring shown in table 5.6 were estimated assuming that the aircraft conducted a successful flight attempt in mission one.

Table 5.6: Missions Score estimation

Score parameter	Mission 1	Mission 2	Mission 3	Ground mission
UDC team mission time	-	70 sec	-	90 sec
Minimum Mission time	-	60 sec	-	60 sec
Number of laps	-	-	6	-
Mission score	1	1.62	2.6	.67
Total mission score			5.98	
Report score			80	
Total score			472	

5.6 Drawing Package

The following drawing package illustrates the 3-view drawing with each part dimensions, the structural arrangement drawing as well as the systems layout drawing, the banner deployment and releasing mechanism and passengers and luggage compartments drawing.



	14/02/2020	Cairo University		
drawn by:	UDC Egypt			
Eman Nabil	SIZE	B	3-VIEW DRAWING	
checked by:				
Mohamed Hetta	SCALE:	1:10	WEIGHT: 17.32 lbs	SHEET 1 OF 4

4

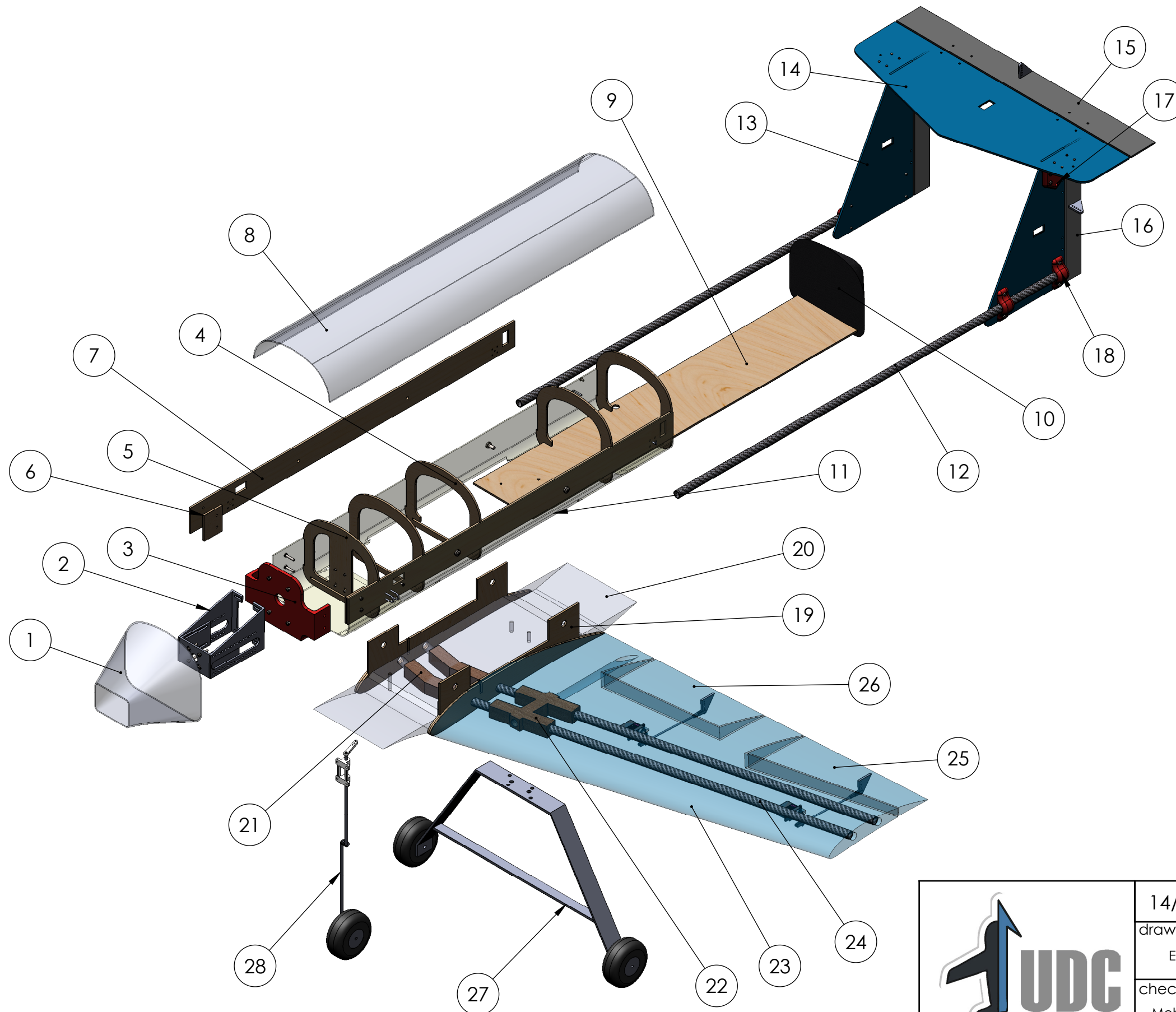
3

2

1

B

B



No.	Part Name	Material	Qty.
1	Nose	Carbon Fiber	1
2	Motor Mount	Aluminum	1
3	Firewall	ABS Plastic	1
4	BulkHead	Plywood	4
5	Nose Gear Mount	Plywood	1
6	Firewall Support	Plywood	2
7	Fuselage Side Wall	Plywood	2
8	Fuselage Upper Skin	Carbon Fiber	1
9	Fuselage Floor	Plywood	1
10	Fuselage Rear Cover	Carbon Fiber	1
11	Fuselage Lower Skin	Carbon Fiber	1
12	Tail Boom	Carbon Fiber	2
13	V-Stabilizer	Plywood	2
14	H-Stabilizer	Plywood	1
15	Elevator	Plywood	1
16	Rudder	Plywood	2
17	V-H Joint	ABS Plastic	2
18	Boom Holder	ABS Plastic	4
19	W-F Connection Plate	Plywood	2
20	Mid-Wing Section	Blue Foam	1
21	Spars Support	Paxolin	2
22	Spars-Boom Connector	Paxolin	2
23	Wing Foam Core	Blue Foam	2
24	Spar	Carbon Fiber	4
25	Aileron	Blue Foam	2
26	Flap	Blue Foam	2
27	Main Gear	Aluminum	1
28	Nose Gear	Aluminum	1



14/02/2020

drawn by:

Eman Nabil

checked by:

Mohamed Hetta

Cairo University

UDC Egypt

STRUCTURAL ARRANGEMENT

SCALE: 1:6 WEIGHT: 7.43 lbs SHEET 2 OF 4

4

3

2

1

4

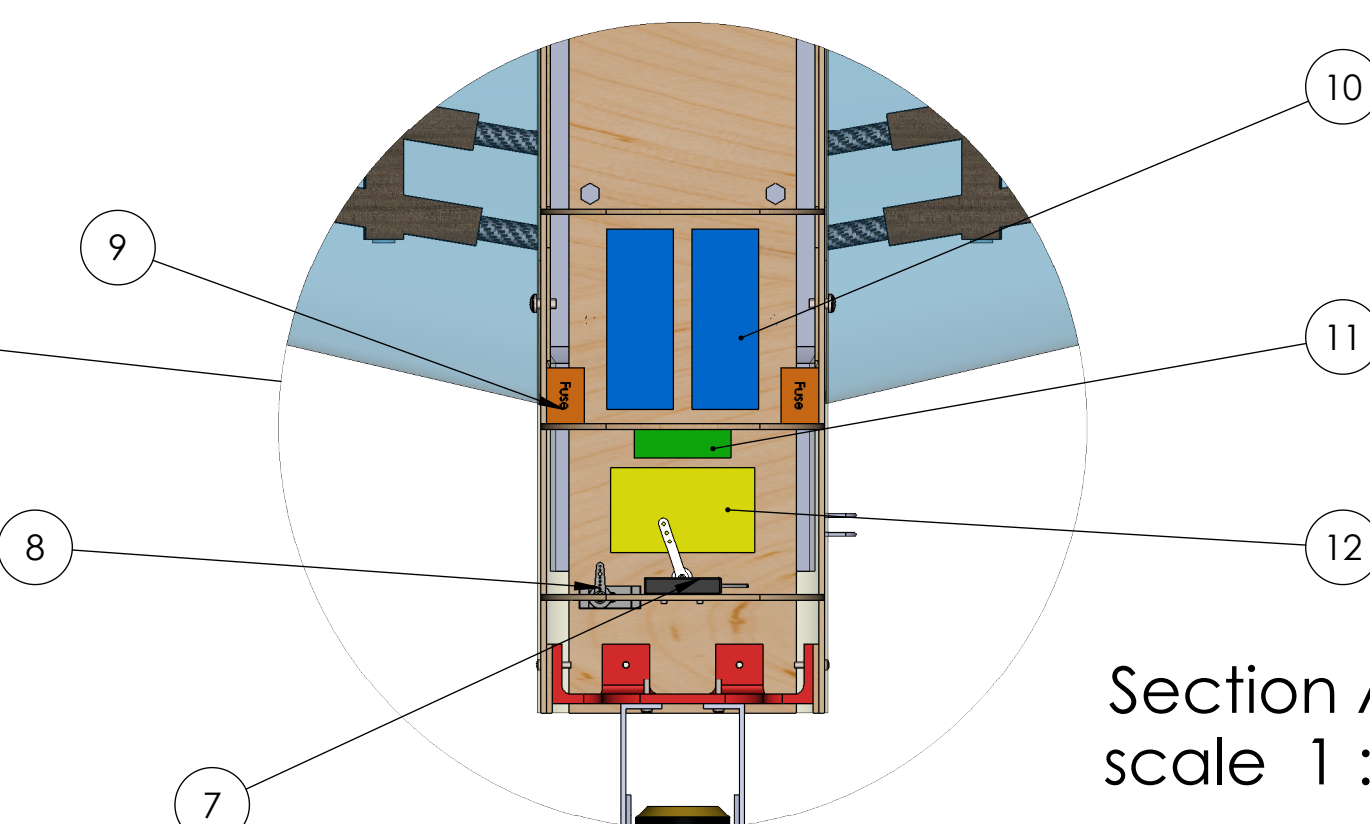
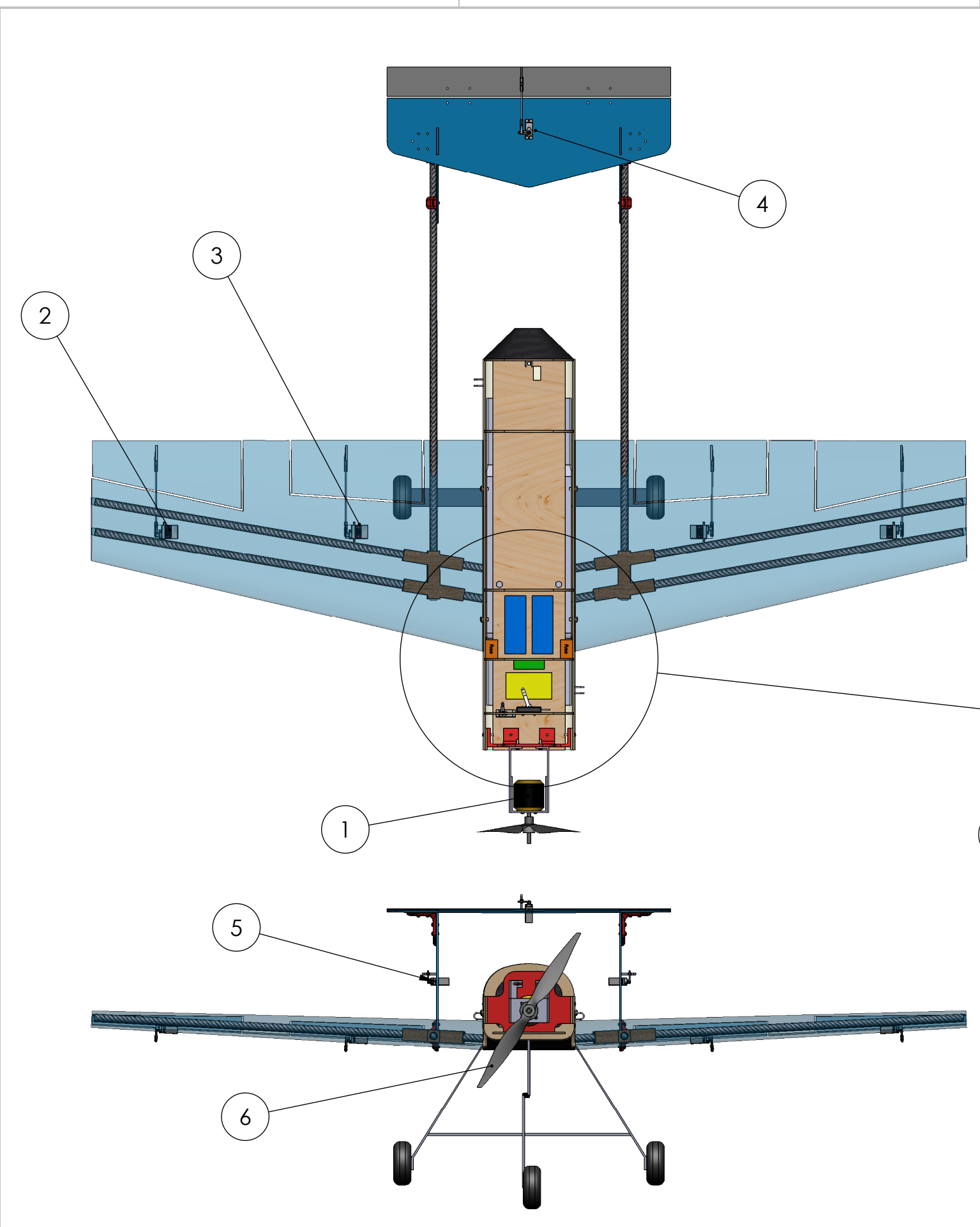
3

2

1

B

B



Section A
scale 1 : 4

	14/02/2020	Cairo University		
	drawn by:	UDC Egypt		
	Eman Nabil			
	checked by:	Mohamed Hetta		
B		SYSTEMS LAYOUT		
SCALE: 1:8		WEIGHT: 10.2 lbs		SHEET 3 OF 4

4

3

2

1

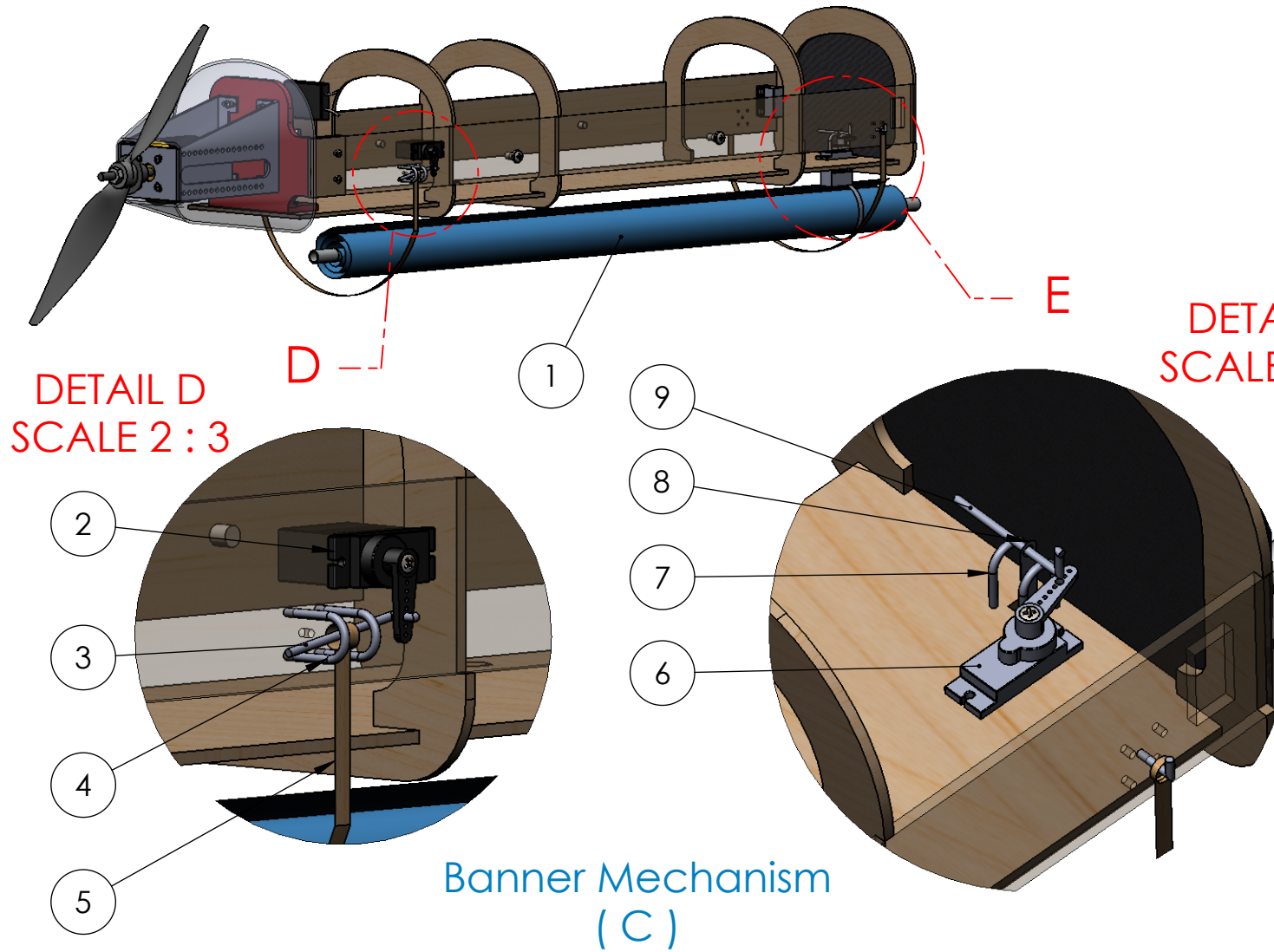
4

3

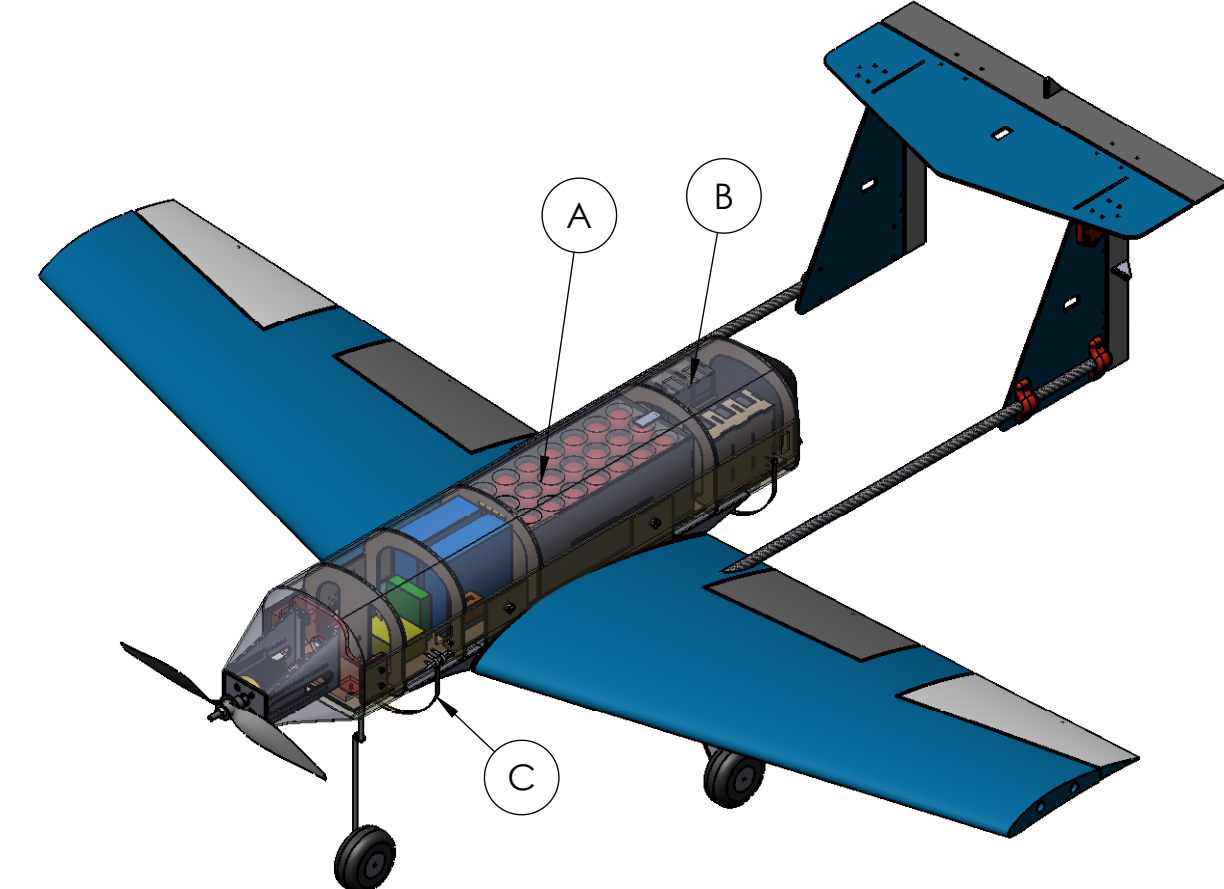
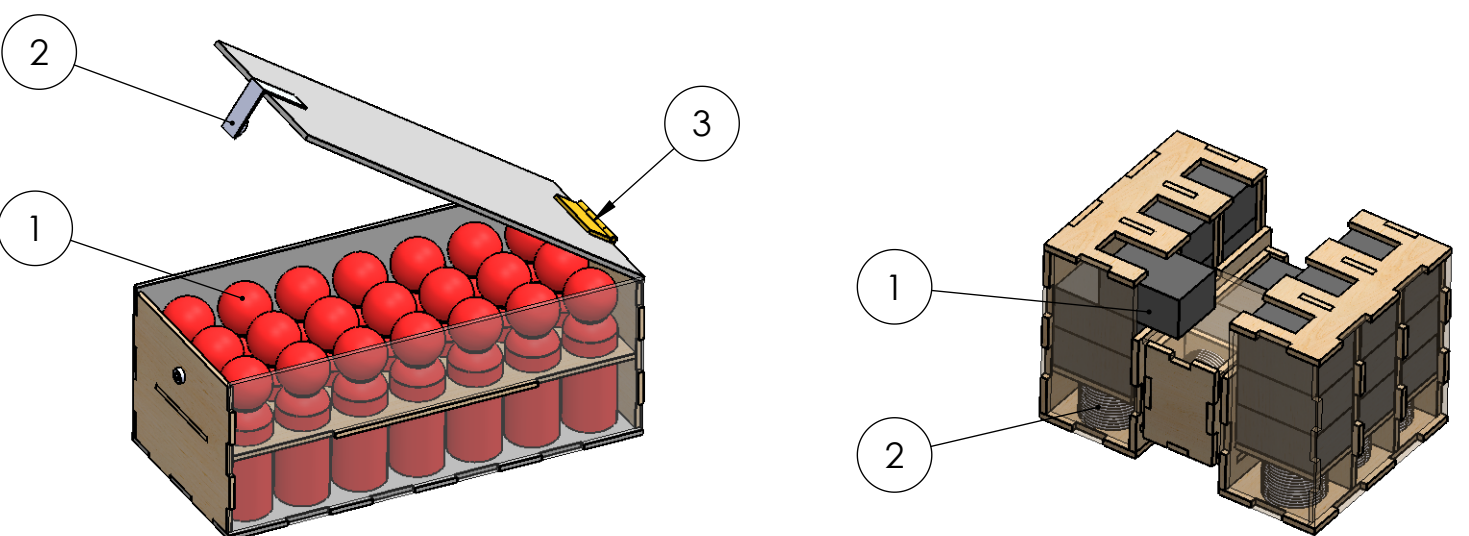
2

1

B



A



Passenger Compartment (A)		
No.	Part Name	Qty.
1	Passenger	18
2	Press Snap Fastner	1
3	Hinge	1

Luggage Compartment (B)		
No.	Part Name	Qty.
1	Luggage	18
2	Spring	7

Banner Mechanism (C)		
No.	Part Name	Qty.
1	Banner	1
2	Deploying Servo	2
3	Rod	2
4	Hook	4
5	Rubber Band	2
6	Releasing Servo	1
7	Hook	2
8	Fishing Line	1
9	Rod	1



14/02/2020

drawn by:

Mohamed Ashraf

checked by:

Mohamed Hetta

Cairo University

UDC Egypt

PAYLOAD ACCOMMODATION

SCALE: N/A WEIGHT: 6.94 lbs SHEET 4 OF 4

4

3

2

1

6.0 Manufacturing Plan

In order to optimize the construction of the aircraft and ensure that it satisfies the structural requirement, several manufacturing processes and materials were evaluated in terms of their weight, strength, manufacturability and cost. Those parameters were prioritized as shown in table 6.1. The main target was to produce a light weighted aircraft that can endure the flight stresses using the minimum amount of resources and cost. The manufacturing time and complicity were also reviewed as highly affecting parameters.

Table 6.1 Manufacturing Factors Weight

Factor	1	2	3	4	5
Weight					
Cost					
Strength					
Manufacturability					

6.1 Manufacturing Processes Investigated

- **Plywood:** It's a stiff light weighted material that can be easily shape and constructed using CNC laser cutting machines and a variety of adhesives. Well-designed and constructed plywood structures increase the overall integrity. Additionally, the fact that our team has a plenty of experience using it made it the perfect choice for manufacturing most of the aircraft parts especially those subjected to a lot of stresses.
- **Foam:** It is a light flexible material which can be formed and cut into various shapes using CNC milling and laser cutting machines. Moreover, it is considered to be the cheapest manufacturing technique. Although it is less stiff than other materials, it has proved to be the best in maintenance and prototyping in addition to being a very suitable building technique specifically for wings.
- **3D Printing:** The 3D printing technique makes it possible to manufacture complicated designs and complex mechanisms in a short period of time. On the other hand, structures made with 3D printing have poor strength to weight ratio so it shouldn't be used in the manufacturing of critical parts.
- **Composites:** Composites are incredibly durable with very high strength-to-weight ratio. In addition, they resist compression and don't easily break under tension. Another advantage of composites is their design flexibility they can be made into just about any shape. The disadvantages of this method are the high initial cost and the team limited experience.

6.2 Selected Manufacturing Process

6.2.1 Wing

The wing was manufactured from Polystyrene foam using CNC hot-wire cutter machine. Each semi span was constructed individually and attached to the fuselage with plywood ribs. The structure was supported with 0.63 in diameter carbon fiber front spar and 0.47 in diameter rear spar. In addition, a twin boom each made of 0.63 in diameter carbon fiber rods were attached to the wing using two irregular I-

section connectors which were made out of paxolin sheets. Moreover, those connectors were attached to the spars from the sides and manufactured such that it gives the wing a swept and dihedral angle. Figure 6.1 shows the lower surface of the wing.

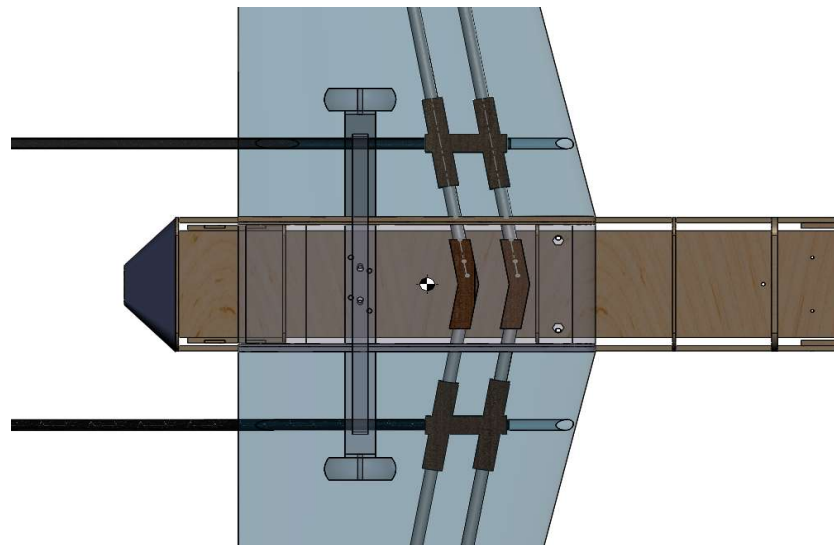


Figure 6.1 Wing Lower Surface

6.2.2 Fuselage and Tail Structure

The fuselage was constructed using plywood due to its high strength to weight ratio. Plywood bulkheads were combined with the fuselage and glued together as shown in figure 6.2 to balance and increase the structural integrity. As shown in figure 6.2, the fuselage skin and cover were made of composite materials which has lighter weight. All parts were assembled together using an epoxy resin. The sides of the fuselage were screwed to wooden ribs connected to the wing and having the airfoil shape. The tail was made of three plywood parts fitted and connected together using bolts and supported using 3D printed L-shaped sections.

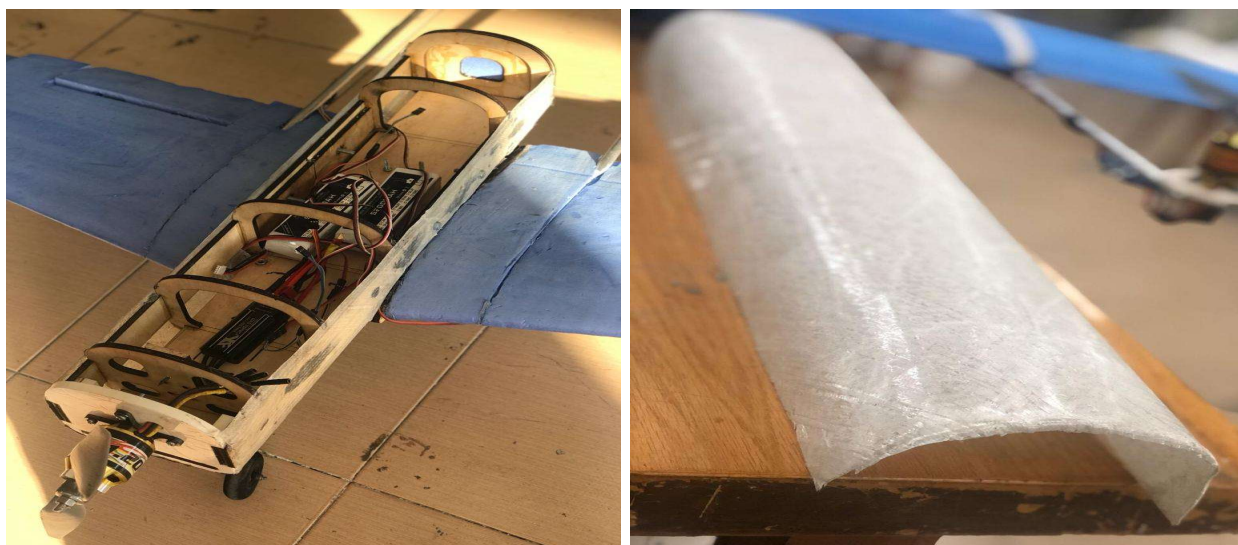


Figure 6.2: Wing Fuselage and Cover

6.2.3 Mechanisms

The passenger was made out of Depron foam boards by cutting the parts using CNC laser cutting machine, while the luggage compartment was manufactured using plywood. The various parts were assembled together using hot glue. The banner deployment and releasing mechanism was made out of balsa wood and metal rods. The manufactured parts are shown in figure 6.4. The passengers were 3D printed each having a bottom hole where steel is inserted to achieve the required weight.



Figure 6.4: Compartment

6.2.4 Banner

The banner along with its stabilizing system were manufactured out of one big piece of polyester fabric having a low specific weight that was then sewed into the required shape. The banner mast was made out of an aluminum rod with steel rings attached to it. Nylon fishing line was used to tow the banner.



Figure 6.5 Insert Banner Photo

6.3 Manufacturing Milestone

In order to keep the team on track and to organize the manufacture process, a Gantt chart shown in figure 6.6 was made to ensure that all members can efficiently integrate all tasks which allowed for rapid aircraft prototyping and testing.

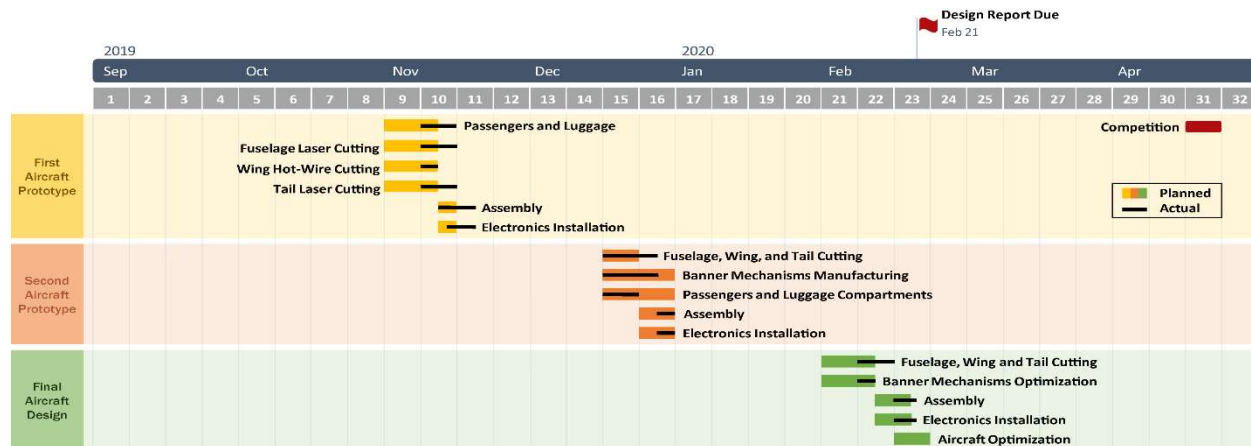


Figure 6.6 Manufacturing Milestone

7.0 Testing Plan

Several tests had been conducted to validate the theoretical calculations. The tests were separated into two main categories, subsystem tests and flight test. Based on the results, final decisions were taken after analysing the results of these tests. Figure 7.1 illustrates our testing procedure.

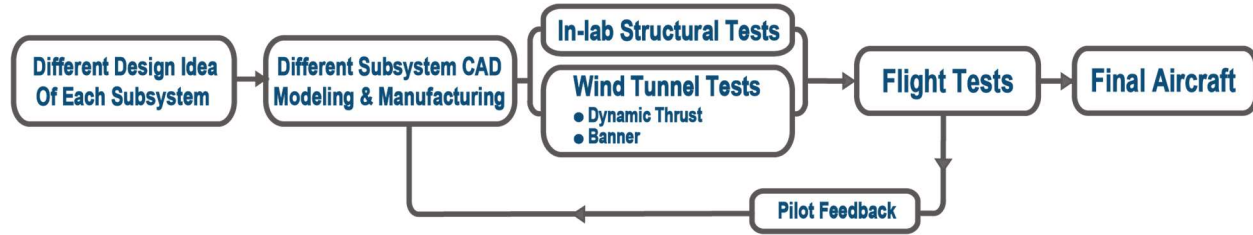


Figure 7.1: Testing Plan Flowchart

7.1 Testing Schedule

The testing schedule shown in Figure 7.1 displays the planned and actual timing of the different tests performed. Our testing plan was designed in an order that the sub-systems were tested in-lab separately. After the sub-systems were insured to be reliable, the whole aircraft is then tested in a real flight test to validate its performance.

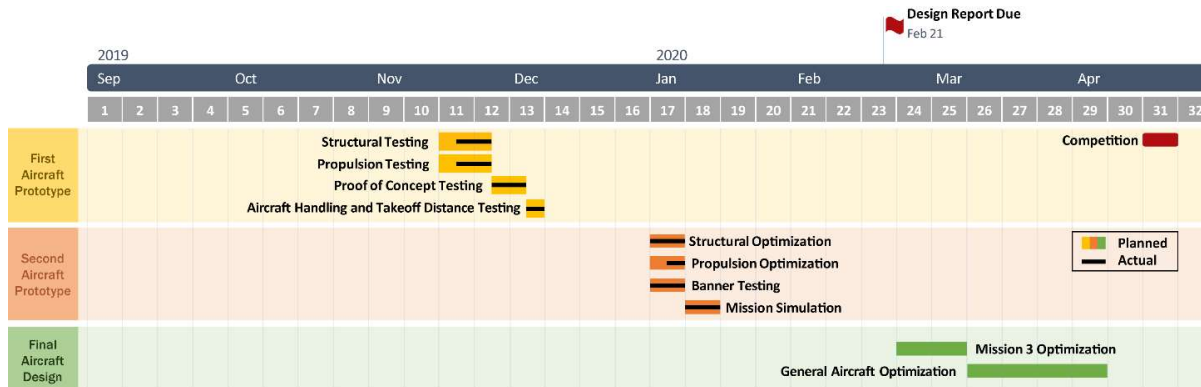


Figure 7.2 Testing Schedule

7.2 Subsystems Testing Objectives

7.2.1 Propulsion Testing

The main objectives of the propulsion testing are confirming the thrust calculation, system efficiency and performance and testing the batteries endurance and performance. Using the testing set up shown in figure 7.3 which consists of thrust bench connected to an ATI Delta F/T sensor in addition to RPM sensor and custom controller that feeds all required data directly to the computer. The propulsion systems considered in section 4.2.2 were tested for actual performance in a wind tunnel at a wide range of velocities. And the thrust, voltage, torque, current draw and RPM were measured. The collected data were then curve fitted, analyzed and compared with the initial values predicted in section 5.3.6.



Figure 7.2 Wind tunnel propulsion system testing

7.2.2 Structural Testing

Wing Testing

A wing bending test was conducted to confirm the structural integrity of the wing design. The structure team conducted load testing that simulated the aerodynamic loads by distributing large load on the wing as shown in Figure 7.4. Spars made of Aluminum, Stainless steel and Carbon Fiber having three different diameters 0.39 in , 0.47 in and 0.62 in each. They underwent a destructive test, which was defined when the team observes excessive deflection, crushing or cracking along the wing. The results showed that the 0.62 in diameter Carbon fiber spar had the least deflection thus largest rigidity. Moreover, it had the largest yield strength. Also a wing tip test was performed on the fully equipped aircraft with all the payloads and passengers.



Figure 7.4: Wing Bending Test

Landing Gear Testing

A drop test shown in figure 7.5 was conducted to assure that the landing gear would be able to endure the load of the aircraft during landing impact. This fully loaded aircraft was dropped from an initial height that was gradually increased until the test fails at 11.8 in . This type of test showed landing gear rigidity, strength and reliability to endure the impact loads. In addition, a taxiing test was conducted to ensure the controllability of the aircraft steering.



Figure 7.5 Landing Gear Drop Test

Firewall Testing

The motor attached to the firewall was mounted on a custom-built testing rig and underwent a throttle test. Different modes of throttle were applied; gradual increase, sudden increase and dynamic fluctuating to ensure that the firewall will withstand the applied thrust load.

Boom Testing

The main objective of the boom testing was to choose the boom that would support the tail. Booms made of Carbon Fiber, Aluminum, and Steel were chosen with three different diameters of *0.39 in, 0.47 in, and 0.63 in* each. The spars were supported by wooden box from one end *cantilevered*. At the free edge, weights were hanged gradually and deflection was observed and calculated for each of them. Loads were added gradually up to 11 lb. The results showed that the *0.63 in* Carbon Fiber had the least deflection and largest yield strength.

7.2.3 Banner Testing

The objective of the tests were to validate the empirical formula mentioned in section 4.4.3, find a material that would produce the lowest drag and find the best stabilizer system in order to minimize the flutter effect. Researches were made to find the common materials used in banners, which were polyester, cotton, and nylon. Polyester proved to be the popular choice and hence wind tunnel tests were conducted on three different polyester types samples having the same dimensions. Accordingly, the best material was chosen for further testing.

After choosing the best material, two types of stabilizing systems were tested as an attempt to find a configuration that would minimize the banner fluttering; tail sock stabilizer and tail streams. It was found that the tail sock increased the drag of the banner with no observed effect on the fluttering. The tail streams didn't do anything for the fluttering as well. Additionally, fraying was observed on the banner end. Consequently, it was decided that the best option is use the banner with no stabilizing systems. Moreover, a set of tests were conducted on different banner lengths of the chosen design at a wide range of velocities to fit a formula for calculating the banner drag.

Deploying and Releasing Mechanisms Testing

In order to ensure the reliability of the deploying and releasing mechanisms and stimulate their behavior during flight, a wind tunnel test was conducted with a relative air velocity 65.6 ft/s . The test showed that the banner mechanism was reliable as the banner was deployed and released successfully.

7.3 Flight Testing

Several flight tests were performed in order to check the ability of the aircraft to perform all the required missions. During each flight the take-off distance, rate of climb and speeds were collected using onboard devices. In order to determine area of improvements, the collected data along with the pilot's feedback were considered during optimizing and designing of the several prototypes.

The flight tests conducted before the report delivery were six types. The first type is proof of concept test, in which the objective was to verify the thrust to weight ratio and validate the expected cruising speed. Secondly, the aircraft's handling quality was tested in a flight test and overall control authorities were checked. Also, the fully equipped aircraft underwent a take-off test in which the aircraft was expected to take-off in 20 ft . After that the aircraft was put to test in a mimicking flight missions that simulate the three actual missions implied by this year's competition rules.

7.4 Flight Checklists

The pre-flight checklist shown in figure 7.6 was made by the pilot team members. The aircraft was checked according to this list before each flight. This way system malfunctioning risk is reduced. After each landing a post-flight checklist was used to inspect the aircraft condition after each attempt.

<ul style="list-style-type: none"> ▪ Aircraft Name ▪ Weight ▪ Location of C.G (from nose) ▪ Battery 		<ul style="list-style-type: none"> ▪ Location ▪ Wind speed ▪ Temperature ▪ Weather 							
			<table style="width: 100%; border-collapse: collapse;"> <tr> <td style="width: 33%;">sunny</td><td style="width: 33%;">Windy</td><td style="width: 33%;">rains</td></tr> <tr> <td><input type="checkbox"/></td><td><input type="checkbox"/></td><td><input type="checkbox"/></td></tr> </table>	sunny	Windy	rains	<input type="checkbox"/>	<input type="checkbox"/>	<input type="checkbox"/>
sunny	Windy	rains							
<input type="checkbox"/>	<input type="checkbox"/>	<input type="checkbox"/>							
Pre - Flight		Post - Flight							
Aircraft structure	<input type="checkbox"/>	Disarm the power	<input type="checkbox"/>						
Control Surface and servos	<input type="checkbox"/>	Motor Temperature	Cool <input type="checkbox"/> Warm <input type="checkbox"/> Hot <input type="checkbox"/>						
Motor	<input type="checkbox"/>	Battery Temperature	Cool <input type="checkbox"/> Warm <input type="checkbox"/> Hot <input type="checkbox"/>						
Check Prop	<input type="checkbox"/>	ESC Temperature	Cool <input type="checkbox"/> Warm <input type="checkbox"/> Hot <input type="checkbox"/>						
Fixation inside fuselage	<input type="checkbox"/>	structure	Good <input type="checkbox"/> Damaged <input type="checkbox"/>						
Wires	<input type="checkbox"/>	Record time	<input type="checkbox"/>						
C.G position	<input type="checkbox"/>	Record joystick setting	<input type="checkbox"/>						
Ground trim of control surface	<input type="checkbox"/>	<ul style="list-style-type: none"> ▪ Pilot Name ▪ Flight number ▪ Date ▪ Time 							
Fail safe mode	<input type="checkbox"/>								
Range check	<input type="checkbox"/>								

Figure 7.6: Flight Checklist

8.0 Performance

8.1.1 Propulsion System Battery

To calculate the actual performance of the batteries, a total of two 12 cell LiPo battery packs were connected to the motor and completely discharged at constant current of 60 and 80 amperes. The capacity and voltage of each test were plotted in figure 8.1 to find the voltage drop and endurance.

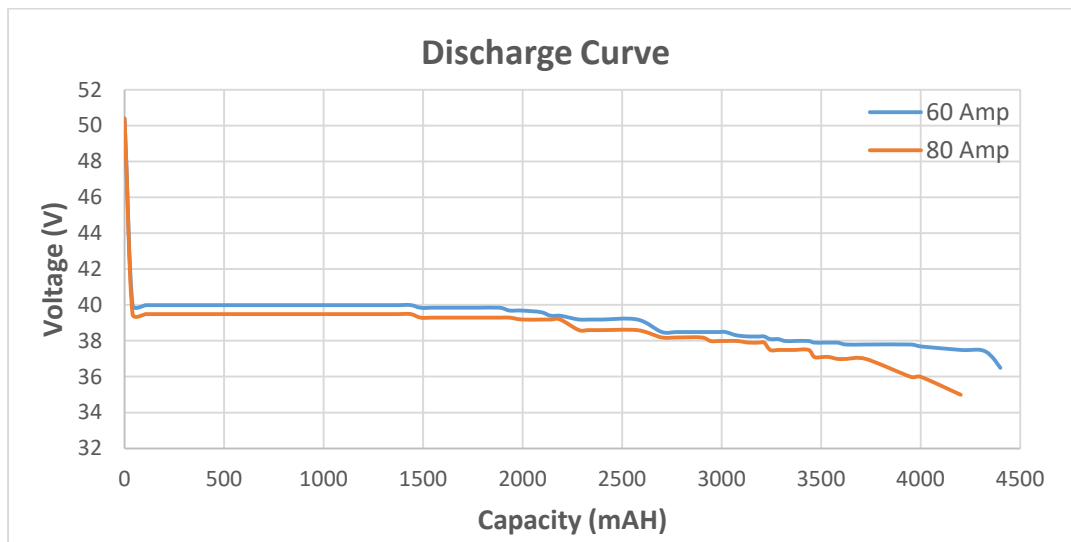


Figure 8.1: Pack Discharge Curve at 10 Ampere

Motors

The actual thrust calculated after conducting the wind tunnel tests on Scorpion HKII-4225 motor along with the APC 12x8 electric propeller combination was compared with the initial thrust predictions. Figure 8.2 shows the difference between the actual and predicted. The error is somehow large and indicated that the thrust values were overestimated. However, the team took such differences in consideration during the optimization process.

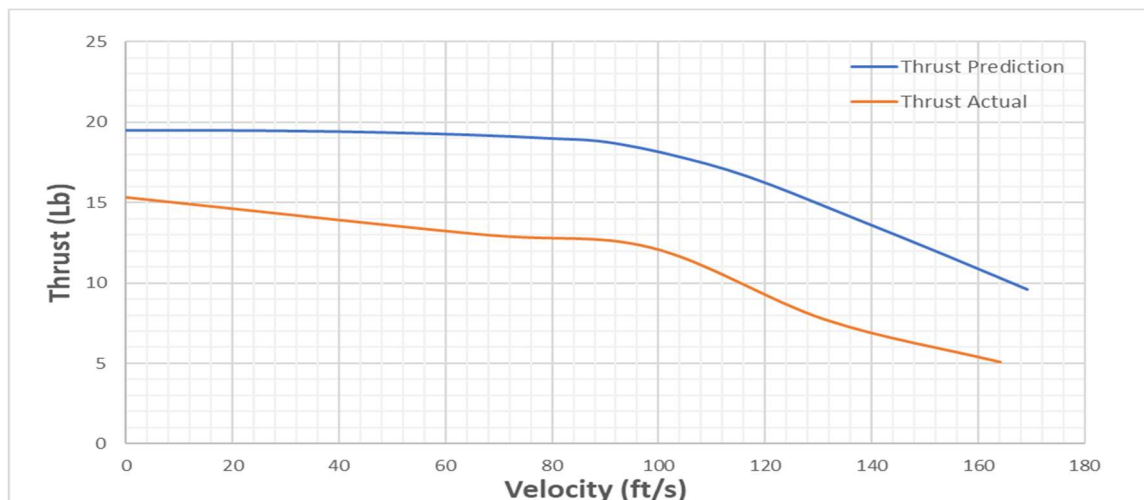


Figure 8.2: Predicted vs. Actual Thrust

8.1.2 Structure Performance

Wing Performance

test bench was installed in order to check the wing semi span ability to carry the applied high loads during the high cruise speed. Concentrated and distributed loads were increased gradually, then the test was repeated to make sure of the wing durability against the dynamic loads.

Also, the aircraft with its maximum takeoff weight in mission 2 underwent a wing tip test as stated in AIAA DBF 20 rules in the technical inspection instructions with acceptable wing deflection.

Banner Deploying and Releasing Mechanism

The banner mechanism showed an obvious reliability with its twin working stages the deploying stage and the releasing stage. The banner mechanism that is totally depending on high torque servomotors which is attached to fuselage and the fishline connection between the servomotors and banner rod were tested in the wind tunnel and the mechanism combination had endured double the expected aerodynamic load due to banner drag in mission 3.

8.2. Demonstrated Flight Performance of the Complete Aircraft

During flight tests phase, the aircraft performance is being compared to the predicted calculated performance. Moreover, verified to be airworthy and capable to perform the three missions successfully.

The following table illustrates the objective of each test, problems encountered and their solutions:

Table 7.1: Flight Test Performance

Test	Observations	Modifications
Proof of Concept	<ul style="list-style-type: none"> - Thrust to weight ratio was sufficient. - Cruising speed was less than expected. - There was a steering problem in the nose landing gear. 	<ul style="list-style-type: none"> - Adjusting the steering mechanism and nose wheel. - Optimizing the fuselage outer shape.
Aircraft handling quality	<ul style="list-style-type: none"> - Aircraft was not responsive enough to the control surfaces. 	<ul style="list-style-type: none"> - Increasing the control surfaces deflection angles. - Resizing the control surfaces.
Take-off distance	<ul style="list-style-type: none"> - The aircraft outstandingly performed the take-off in a shorter distance than expected. 	<ul style="list-style-type: none"> - N/A
Mission 1	<ul style="list-style-type: none"> - Phenomenal torque roll was observed, as the motor's torque was high 	<ul style="list-style-type: none"> - Increasing the rudder area. - Using a gyro sensor to auto trim the aircraft at take-off
Mission 2	<ul style="list-style-type: none"> - The flaps performed well during take-off. - Cruising speed was less than expected 	<ul style="list-style-type: none"> - Modify the propulsion system configuration.
Mission 3	<ul style="list-style-type: none"> - The fluttering effect made the aircraft yaws during cruising significantly and required continuous trimming 	<ul style="list-style-type: none"> - Decreasing the fluttering effect of the banner. - Add damping spring on the hinge holding the banner.
Additional	<ul style="list-style-type: none"> - Further tests will be conducted after report delivery 	

After attempting flight tests mocking the three missions and performing them successfully, the following table summarizes the comparison between flight tests results and the predict values:

Table 7.2: Actual vs. Predicted Performance

Performance Parameter	Mission 1		Mission 2		Mission 3	
	Predicted	Actual	Predicted	Actual	Predicted	Actual
Take-off distance (ft.)	18	14.8	29.53	37.7	18	16.5
Rate of climb (ft/s)	19.7	13.5	11.5	8.2	16.4	13
V_{Cruise} (ft/s)	82	75	147.6	112	82	64
V_{Turn} (ft/s)	65.6	53	60.7	57.4	55.8	52.6
Lap Time (Sec)	30	35	23	29	32	43



Figure 8.3: Aircraft Flight Testing

9.0 Bibliography

- [1] "APC-Propellers-DL-Model" <https://github.com/AhmedHisham1/APC-Propellers-DL-Model>
- [2] R. A. Fairthorne , "Drag of Flags", Reports and Memoranda, May 1930 http://emmanuel-virot.weebly.com/uploads/9/4/5/6/9456170/fairthorne_1930_-_drag_of_flags.pdf
- [3] Raymer, Daniel. P., Aircraft Design: A Conceptual Approach, 4th edition Reston, VA: American Institute of Aeronautics and Astronautics, 2006.
- [4] "MIT Open Courseware", Basic Aircraft Design Rules, 2006. [Online],
<https://ocw.mit.edu/courses/aeronautics-and-astronautics/16-01%20-unified-engineering-i-ii-iii-iv-fall-2005-spring-2006/systems-labs-06/>
- [5] Nelson, Robert. C., Flight Stability and Automatic Control, 2nd edition, McGraw-Hill, New York, 1998.
- [6] APC Prop, " APC Propeller Performance Data " <https://www.apcprop.com/technical-information/performance-data/>
- [7] J.B. Brandt, R.W. Deters, G.K. Ananda, and M.S. Selig, UIUC Propeller Database, University of Illinois at Urbana-Champaign, 25/10/2019 <https://m-selig.ae.illinois.edu/props/propDB.html>
- [8] AIAA Student Design Build Fly, "2019-20 DBF Q&A 1," 2018-2019. [Online]. Available:
<https://www.aiaa.org/dbf/competition-information/FAQ>
- [9] "Pro advices", Gudmundsson, Design handbook Aircraft Preliminary, Great Owl Publishing, 2011.
- [10] Staples, Gabriel, "Propeller Static & Dynamic Thrust Calculation" [online Article],
<https://www.electricrcaircraftguy.com/2014/04/propeller-static-dynamic-thrust-equation-background.html>, [written April 12, 2014]
- [11] Sadraey, Mohammad. H., Aircraft Design: A Systems Engineering Approach, 1st edition, John Wiley & sons, USA, 2013.
- [12] Gundlach, Jay, "Designing Unmanned Aircraft Systems: A Comprehensive Approach", 2nd edition Reston, VA: American Institute of Aeronautics and Astronautics, 2014.